

UNCLASSIFIED

AD NUMBER
AD816123
NEW LIMITATION CHANGE
TO Approved for public release, distribution unlimited
FROM Distribution authorized to U.S. Gov't. agencies and their contractors; Critical Technology; MAY 1967. Other requests shall be referred to Air Force Materiels Laboratory, Attn: Metals and Ceramics Division, Wright-Patterson AFB, OH.
AUTHORITY
WRDC/IST ltr dtd 21 Mar 1989

THIS PAGE IS UNCLASSIFIED

THIS REPORT HAS BEEN DELIMITED
AND CLEARED FOR PUBLIC RELEASE
UNDER DOD DIRECTIVE 5200.20 AND
NO RESTRICTIONS ARE IMPOSED UPON
ITS USE AND DISCLOSURE.

DISTRIBUTION STATEMENT A

APPROVED FOR PUBLIC RELEASE;

DISTRIBUTION UNLIMITED.

AFML-TR-65-2
Part III, Volume II

AD 816123

TERNARY PHASE EQUILIBRIA IN TRANSITION METAL-BORON-CARBON-SILICON SYSTEMS

**PART III. SPECIAL EXPERIMENTAL TECHNIQUES
VOLUME II. A PIRANI-FURNACE FOR THE PRECISION
DETERMINATION OF THE MELTING TEMPERATURE OF
REFRACTORY METALLIC SUBSTANCES**

*E. RUDY
G. PROGULSKI*

AEROJET-GENERAL CORPORATION

TECHNICAL REPORT No. AFML-TR-65-2, PART III, VOLUME II

MAY 1967

This document is subject to special export controls and such transmittal to foreign governments or foreign nationals may be made only with prior approval of Metals and Ceramics Division, Air Force Materials Laboratory, Wright-Patterson Air Force Base, Ohio.

AIR FORCE MATERIALS LABORATORY
RESEARCH AND TECHNOLOGY DIVISION
AIR FORCE SYSTEMS COMMAND
WRIGHT-PATTERSON AIR FORCE BASE, OHIO



**Best
Available
Copy**

NOTICES

When Government drawings, specifications, or other data are used for any purpose other than in connection with a definitely related Government procurement operations, the United States Government thereby incurs no responsibility nor any obligation whatsoever; and the fact that the Government may have formulated, furnished, or in any way supplied the said drawings, specifications, or other data, is not to be regarded by implication or otherwise as in any manner licensing the holder or any other person or corporation, or conveying any rights or permission to manufacture, use, or sell any patented invention that may in any way be related thereto.

Copies of this report should not be returned to the Research and Technology Division unless return is required by security considerations, contractual obligations, or notice on a specific document.

**TERNARY PHASE EQUILIBRIA IN TRANSITION
METAL-BORON-CARBON-SILICON SYSTEMS**

**PART III. SPECIAL EXPERIMENTAL TECHNIQUES
VOLUME II. A PIRANI-FURNACE FOR THE PRECISION
DETERMINATION OF THE MELTING TEMPERATURE OF
REFRACTORY METALLIC SUBSTANCES**

*E. RUDY
G. PROGULSKI*

This document is subject to special export controls and each transmittal to foreign governments or foreign nationals may be made only with prior approval of Metals and Ceramics Division, Air Force Materials Laboratory, Wright-Patterson Air Force Base, Ohio.

FOREWORD

The research described and illustrated in this report was performed at the Materials Research Laboratory, Aerojet-General Corporation, Sacramento, California under USAF Contract No. AF 33(615)-1249. The contract was initiated under Project No. 7350, Task No. 735001. The work was administered under the direction of the Air Force Materials Laboratory, Research and Technology Division with Lt. P.J. Marchiando acting a Project Engineer, and Dr. E. Rudy, Aerojet-General Corporation as Principal Investigator. Professor Dr. Hans Nowotny, University of Vienna, Austria, served as consultant to the project.

The project, which includes the experimental and theoretical investigation of selected refractory ternary systems in the system classes Me_1-Me_2-C , $Me-B-C$, Me_1-Me_2-B , $Me-Si-B$ and $Me-Si-C$ was initiated on 1 January 1964. The furnace described was developed and built on Company funds in support of the above program.

The design and development work was carried out by E. Rudy and G. Progulski. Messrs St. Maskiewicz and T. Eckert were of assistance in the design of the power supply.

The help of Mr. R. Cristoni in preparing the drawings, and of Mrs. J. Weidner, who typed the report, is gratefully acknowledged.

The manuscript of this report was released by the authors September 1966 for publication as an RTD Technical Report.

Other reports issued under USAF Contract AF 33(615)-1249 have included:

Part I. Related Binary System

- Volume I. Mo-C System
- Volume II. Ti-C and Zr-C Systems
- Volume III. Mo-B and W-B Systems
- Volume IV. Hf-C System
- Volume V. Ta-C System
- Volume VI. W-C System. Supplemental Information on the Mo-C System
- Volume VII. Ti-B System
- Volume VIII. Zr-B System
- Volume IX. Hf-B System
- Volume X. V-B, Nb-B, and Ta-B Systems

Part II. Ternary Systems

- Volume I. Ta-Hf-C System
- Volume II. Ti-Ta-C System
- Volume III. Zr-Ta-C System
- Volume IV. Zr-Hf-C, Ti-Hf-C, and Ti-Zr-C Systems

FOREWORD (Cont'd)

- Volume V. Ti-Mo-B System
- Volume VI. Zr-Hf-B System
- Volume VII. Ti-Si-C, Nb-Si-C, and W-Si-C Systems
- Volume VIII. Ta-W-C System
- Volume IX. Zr-W-B System. Pseudobinary Systems
TaB₂-HfB₂
- Volume X. The Systems Zr-Si-C, Hf-Si-C, Zr-Si-B,
and Hf-Si-B

- Volume XI. Hf-Mo-B and Hf-W-B Systems
- Volume XII. Ti-Zr-B System. Pseudobinary Systems
ZrB₂-NbB₂, ZrB₂-TaB₂, and HfB₂-NbB₂
- Volume XIII. Phase Diagrams of the Systems Ti-B-C,
Zr-B-C, and Hf-B-C

Part III. Special Experimental Techniques.

- Volume I. High Temperature Differential Thermal
Analysis

Part IV. Thermochemical Calculations

- Volume I. Thermodynamic Properties of Group IV, V, and
VI Binary Transition Metal Carbides.
- Volume II. Thermodynamic Interpretation of Ternary
Phase Diagrams
- Volume III. Computational Approach to the Calculation of
Ternary Phase Diagrams.

Final Report: High Temperature Phase Equilibria in Transition Metal-
Boron-Carbon-Silicon Systems.

This technical report has been reviewed and is approved.



W. G. RAMKE
Chief, Ceramics and Graphite Branch
Metals and Ceramics Division
Air Force Materials Laboratory

ABSTRACT

An advanced design of a Pirani furnace is presented which allows the precision determination of the melting temperatures of refractory metallic alloys. The method uses resistance heating of a specimen held between two water-cooled electrodes. The temperature of the phase change is determined optically with a disappearing-filament type micropyrometer at a small hole located in the center of the sample. Temperature calibration procedures, as well as methods and tools for the specimen preparation, are discussed. Measurements of the melting points of refractory metals and alloys, as well as of isothermal reaction temperatures in binary metal-carbon and metal-boron systems, are presented and compared with earlier data.

TABLE OF CONTENTS

	PAGE
I. <u>INTRODUCTION</u>	1
II. <u>LITERATURE REVIEW</u>	3
III. <u>FURNACE DESCRIPTION</u>	6
A. Design Considerations and Physical Setup	6
B. Power Control	9
C. Operation	12
IV. <u>TEMPERATURE MEASUREMENT</u>	16
A. Pyrometer Calibration	16
B. Correction Terms for Non-Black Body Conditions of the Hole and for Losses in the Quartz Window.	19
C. Secondary Temperature Standards	25
V. <u>PREPARATION OF TEST SPECIMENS</u>	28
VI. <u>MEASUREMENTS</u>	31
A. Melting Points of Refractory Metals	31
B. Solidus Temperatures of Refractory Metal-Carbon Alloys	35
C. Solidus Temperatures of Refractory Metal-Boron Alloys	35
D. Maximum Solidus Temperatures of the Tantalum Hafnium Monocarbide Solid Solution	40
VII. <u>DISCUSSION</u>	46
References	48

LIST OF ILLUSTRATIONS

FIGURE		PAGE
1	Sectional View of the Pirani Melting Point Furnace	7
2	Lateral Specimen Clamping in the Pirani Furnace	8
3	Interior View of the Melting Point Furnace, Showing Stationary and Adjusting Electrode, and the Lateral Specimen Clamping Assembly	2
4	Face-to-Face Clamping of the Test Specimen, and Gravity Balance System.	9
5	Power Supply and Control System for the Melting Point Furnace	11
6	View Through the Observation Window at a Melting Point Specimen at Temperature	13
7	Typical Appearance of a Pirani Melting Point Specimen After Melting.	14
8	Sectioned Porous Melting Point Sample After Incipient Melting was Noted	14
9	Typical Melting Behavior Observed with the Pirani-Technique	15
10	Temperature Correction Chart for the Pirani Furnace	21
11	Graphite Die and Heater Components for Hot Pressing Bar-Shaped Melting Point Specimens	29
12	Pirani Melting Point Specimen, Hot Pressed and Ground to Shape	29
13	Shaped Die with Retractable Center Pin for Cold Pressing Melting Point Specimens	30
14	Melting Point Specimen, Cold Pressed in the Shaped Die Assembly Shown in Figure 13	30
15	Maximum Solidus Temperatures for the Solid Solution ($T_s, H^{\circ}C_{1-x}$)	45

LIST OF TABLES

TABLE		PAGE
1	Temperature Uncertainties in the NBS Certified Standard Pyrometers and the Tungsten Ribbon-Filament Lamps	18
2	Overall Temperature Uncertainties for the Micro-Optical Pyrometers	18
3	Mean Emissivity Coefficient of Black Body Holes in Metallic Specimens (Rough Surface).	20
4	Effect of the Number of Quartz Windows ($d = 5$ mm) Upon the Apparent Temperatures of a Black Body Source	24
5	Fixed Temperature Points (New International Scale, 1949)	25
6	Secondary High Temperature Reference Points Based on Eutectic Reactions	27
7	Secondary Temperature Standards, Based on Solid State Reactions	27
8	Melting Points of Refractory Metals	32
9	Chemical Analysis of the Group V Metal Powders	34
10	Congruent Melting Points of Cubic (B1) Refractory Monocarbides	36
11	Maximum Solidus Temperatures of Selected Carbide Phases	37
12	Metal + Metal Carbide Eutectic Reaction Isotherms	38
13	Metal Carbide + Graphite Eutectic Reaction Isotherms	39
14	Maximum Solidus Temperatures of Group IV Metal Borides	41
15	Maximum Solidus Temperatures of Group V Metal Borides	42
16	Maximum Solidus Temperatures of Group VI Metal Borides	43
17	Metal-Boride Eutectics	44

I. INTRODUCTION

Apart from the difficulties associated with the construction of furnaces capable of operating under controlled conditions at high temperatures, and the problems involved in the precise measurement of high temperatures, one of the major problems in the precision determination of the melting temperatures of refractory substances is posed by the interaction of the test sample with its environment. The latter specifically concerns chemical interactions with the container materials, still used in the majority of current melting point techniques; adequate precautions usually can be taken to prevent contamination from the furnace atmosphere.

It is considered a comparatively simple task to find materials of sufficient inertness to serve as crucible material for many lower-melting elements and alloys; this is understandable, since large differences between the melting temperatures of sample and container material tend to shift the eutectic composition close to that of the lower melting phase, while the eutectic temperatures approach the true melting point. Many oxides, such as zirconia, hafnia, thoria, alumina, etc. are available which possess, in addition to high melting points, high stability with respect to interaction products; they have, therefore, been the most widely used container materials in melting point studies.

Other materials, sometimes employed, include graphite for non-carbide forming alloys, certain refractory transition metals such as tantalum and tungsten for measurements on rare-earth metal alloys, and of boron nitride in selected applications. It should be realized however, that the data obtained by this method do not represent the true melting point, but correspond to the minimum (mostly eutectic) solidus temperatures existing between the given combinations; their quality is thus dependent upon the skill of the investigator in choosing such combinations of test and container material which will give him the least falsification of the test results.

Other related techniques sometimes employed, such as suspending the test specimens from metal wires or graphite threads, etc., generally

suffer from the same shortcomings and are likely to produce erroneous results when applied to higher melting alloys.

The container as well as the suspending technique fail for obvious reasons in the study of refractory alloys: Besides chemical incompatibility, many of the refractory alloys or compounds of technical interest, such as the carbides, borides, and silicides, for example, have melting temperatures exceeding those of the most refractory oxides, and approaching the sublimation point of graphite.

In 1923, M. Pirani and H. Alterthum⁽¹⁾ described a furnace which essentially eliminates the interaction problem. The principle of the method is simple: A bar-shaped specimen which is clamped between two water-cooled electrodes, is heated resistively to the temperature of the phase change. A small black body hole, located in the center of a narrowed portion of the specimen, serves as the reference point for the optical temperature measurements. Determination of the melting points of selected high-melting alloys, carried out with this apparatus in subsequent years by C. Agte and H. Alterthum^(2, 3), proved this technique to be extremely valuable and capable of high accuracy, and their data, determined now over thirty years ago, still must be considered as being among the most precise available to date. Although the method had been nearly forgotten over the following two decades, increased interest in the refractory alloys in recent years has revived interest in its use and further development.

The present report describes a refined version of a Pirani-type melting point furnace, which was developed in the time period 1963-1964 at the Aerojet Materials Research facilities in conjunction with studies of the high temperature phase relationships in refractory alloys systems. Since the time it was put in operation, a large number of measurements on refractory alloys have been carried out and the device has proven itself a very effective tool for high temperature phase diagram studies.

II. LITERATURE REVIEW

A detailed account and discussion of the numerous techniques and apparatus used for previous melting point studies would exceed the scope of the report, and the reader may be referred to special texts available on this subject⁽⁴⁾. Since the apparatus to be described has been designed, and was primarily used, for measurements on very refractory alloys, we shall restrict the review to a discussion of previous high temperature methods.

We may, arbitrarily, separate currently used techniques into two categories: techniques, which require the use of a container or some other support for the test specimen, and methods, which essentially operate on a containerless principle.

In the first method the sample and container assembly is heated by radiation or conduction from a heating element in resistance-type, or from the susceptor in induction-type furnaces. Melting is either observed visually through a pyrometer, or the phase change is indicated by discontinuities in the output of suitable temperature transducers.

In the apparatus described by R. Kieffer and co-workers⁽⁵⁾ a small piece of the test sample is positioned in a tantalum cup, which is supported on top of a thin tungsten rod. To avoid or retard interaction, a thin layer of refractory oxide or other material is usually placed between the sample and the support material. The specimen assembly is mounted inside a thin-walled tungsten tube, which is resistively heated between two water-cooled copper electrodes. Sample temperatures are measured pyrometrically through a quartz port in the furnace wall and a small hole in the heating element. The temperature, where the first signs of melt become apparent at the specimen surface, is taken as being representative for the melting or solidus point.

Kieffer's method, which later, in a refined version, has been used by B. Riley⁽⁶⁾ for melting point measurements on refractory alloys and selected oxides, has the advantage of requiring only small amounts of sample material.

The technique is well suited for melting point measurements on metals or metal alloys, which form complete solid solutions with the higher melting tantalum (for example molybdenum, niobium, titanium) or, by virtue of the large melting point and stability differences, for lower melting alloys (iron and platinum metals) which do not appreciably interact with refractory oxides, such as thoria. It is not applicable to very reactive metal alloys (hafnium, zirconium) and for the determination of the melting points of silicide, carbide and boride phases, for which either no compatible support materials can be found, or their melting points exceed the temperature capability of the furnace ($\sim 3100^{\circ}\text{C}$).

Graphite has frequently been used as a sample container material for investigations in carbide systems^(6, 7, 8). In this specific application, advantage is taken of the fact, that the metal carbide + graphite eutectic temperatures are usually much higher than the melting isotherms in the metal-rich regions of these systems, and transport of carbon through the carburized layers is sufficiently slow to allow time for the measurements. Melt formation is either analysed for by post-experiment metallographic inspection of the alloys after exposure at a series of temperatures^(6, 7, 8, 9), or by direct pyrometric observations^(10, 11). Recently developed high temperature DTA-techniques, using either high temperature thermocouples such as boron/boronated graphite⁽¹²⁾ or photoelectric devices^(14, 14, 15) as temperature transducers, may be considered as improved modifications of this technique in this specific application.

Other melting point methods belonging to the first group, and which have been employed for solidus studies in selected binary and ternary metal systems, include heating of the sample in folded tungsten or tantalum ribbon elements⁽¹⁶⁾, in tungsten wire baskets⁽¹⁷⁾, or by suspending the specimen from wires within the tubular heating element of a high temperature furnace.^(18, 19) The limitations of the latter techniques are the same as discussed for Kieffer's apparatus.

Among the containerless operating methods the apparatus described by M. Pirani and H. H. Alterthum⁽¹⁾ is the most versatile and yields the

most reproducible results. In their system, a bar-shaped specimen is clamped between two water-cooled electrodes and heated resistively to the melting or solidus point. A small hole located in the center of a narrowed portion of the sample bar serves as black body reference for the pyrometric temperature measurement. The loss of energy by surface radiation causes a temperature gradient across the specimen, which, depending on the sample configuration and its thermophysical properties, can approach several hundred degrees centigrades at temperatures above 3000°C. Thus, melting is first observed in the interior, while the solid outer shell prevents the sample from collapsing.

The resistively heating method has been extensively used in the early thirties for measurements of the melting points of refractory carbide phases, particularly by C. Agte and H. Alterthurn⁽²⁾ and E. Friedrich and L. Sittig⁽⁵²⁾; more recently, similar furnaces were described by R. I. Jaffee and H. P. Nielson⁽²⁰⁾, E. M. Savitski⁽²¹⁾, R. P. Adams and R. A. Beall⁽²²⁾, H. Kimura and Y. Sasaki⁽²³⁾, C. F. Zalabak⁽²⁴⁾, and A. G. Knapton, et al.⁽²⁵⁾ and used for measurements of the solidus temperatures in refractory alloy systems. A preliminary description of the furnace designed in this laboratory has been given in an earlier report⁽²⁶⁾.

Other techniques, which also may be considered to belong to the second group, are the arc-melting technique described by G. A. Geach and J. D. Summers-Smith⁽²⁷⁾; in their method, the test specimen is partially molten in an arc furnace, and the temperature of the solid-liquid interface is determined pyro-optically through a window in the furnace wall. Difficulties encountered include proper arc-control, preferential vaporation of alloy components due to local overheating, and large temperature uncertainties caused by the generally unknown emissivity coefficients of the radiating surfaces.

Heating of the test specimens in the r²-field of an eddy current concentrator⁽²⁸⁾ also eliminates to a large extent contamination by foreign substances; however, since power dissipation is confined to a thin outer shell of the specimen, the method lacks the benefit of the temperature gradient inherent in the Pirani

technique. Furthermore, concentration changes due to preferential material losses from the surface may result in premature melting of the outer shell and thus not allow the true melting point to be approached.

III. FURNACE DESCRIPTION

A. DESIGN CONSIDERATIONS AND PHYSICAL SETUP

The main emphasis in the design of the apparatus was devoted to speed and convenience of operation, use of only small quantities of sample material, and the specimen clamping arrangement to accept brittle and low-strength specimen without danger of breakage. The resulting design is shown in Figure 1.

The essential parts of the furnace consist of two water-cooled copper electrodes enclosed in a double-jacketed vacuum-tight housing. To allow for thermal expansion as well as for other dimensional changes of the sample while maintaining proper electrical contact during the test run, one electrode is kept movable.

Depending on the type of material and mode of operation, two different ways how the sample is attached to the electrodes are in use: For long-time equilibration treatments of ductile alloy specimens at high temperatures, the bar-shaped specimen is clamped between two tungsten platelets (Figure 2). Firm electrical contact during the experiment is maintained by a constant clamping force, applied through a lever arm by weights (visible in Figure 3 in front of the electrodes).

For the melting point runs, the arrangement shown in the self-explanatory drawing of Figure 4 is used exclusively. The clamping force is made adjustable by means of a gravity balancing system, which is firmly connected outside the furnace chamber to the power feed-through shaft of the movable electrode. The maximum axial force, which can be exerted on the sample is 2000g, and can be controlled to within $\pm 30g$. Sudden axial movements of the self-adjusting electrode during evacuation or pressurization

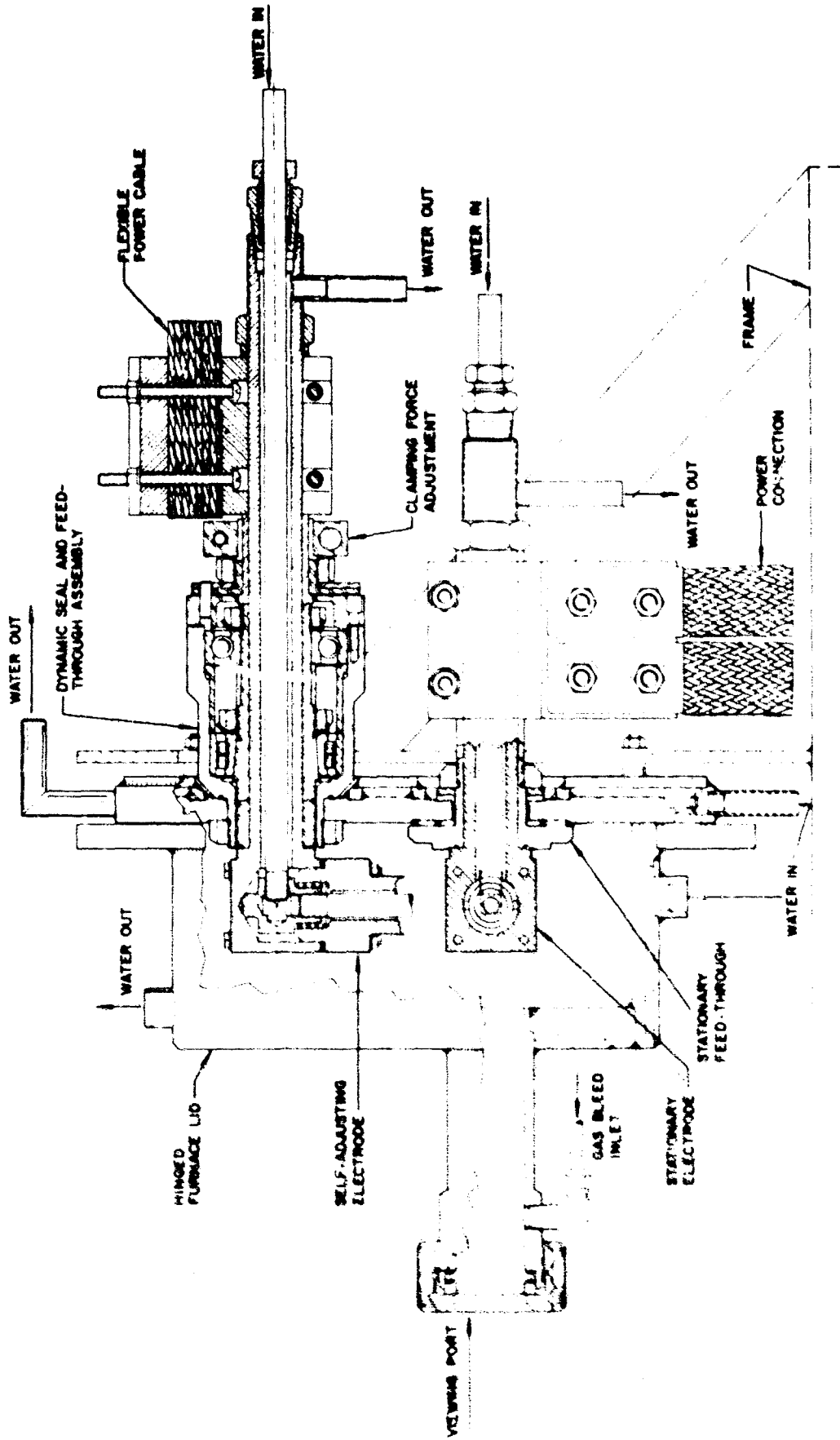


Figure 1. Sectional View of the Pirani Melting Point Furnace.

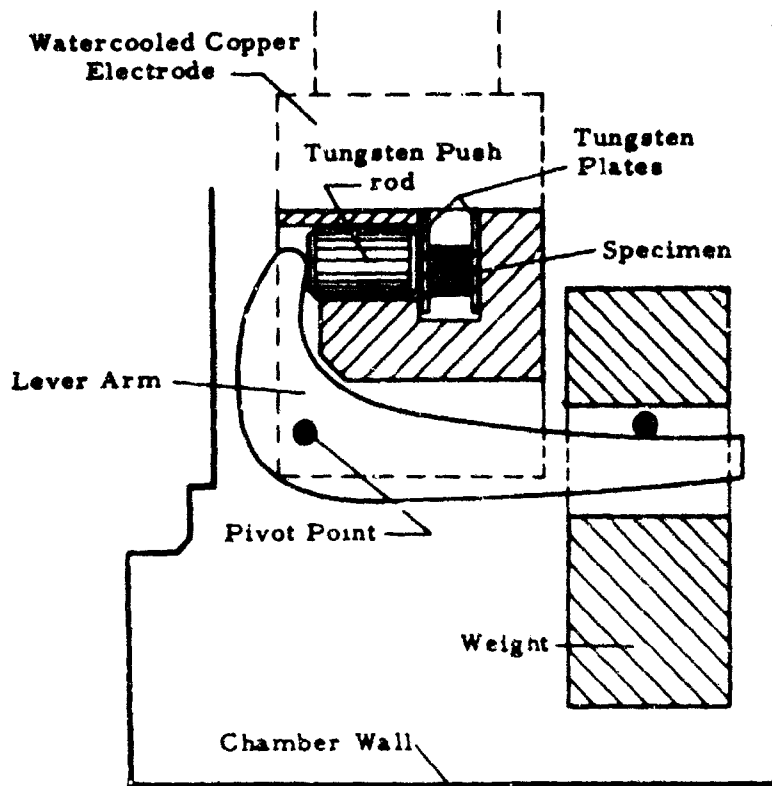


Figure 2. Lateral Specimen Clamping in the Pirani Furnace.

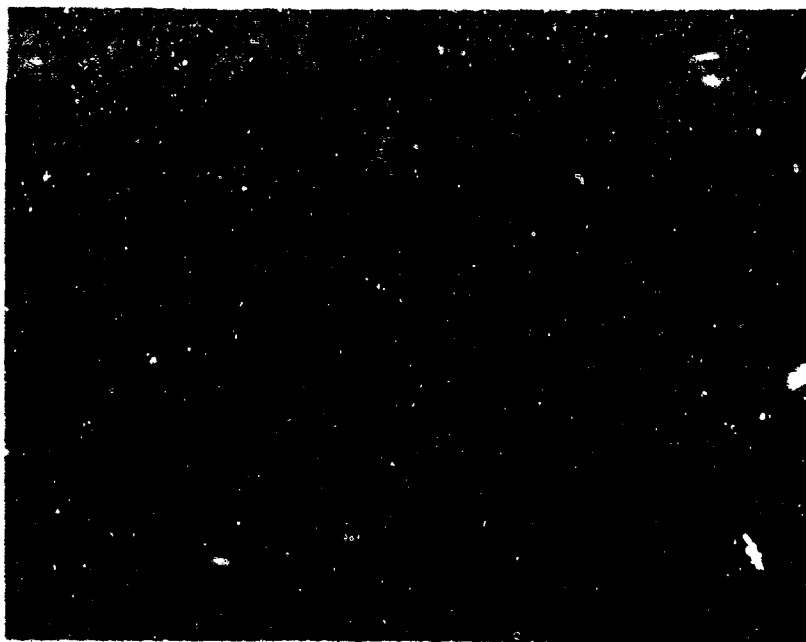


Figure 3. Interior View of the Melting Point Furnace, Showing Stationary and Adjusting Electrode, and the Lateral Specimen Clamping Assembly.

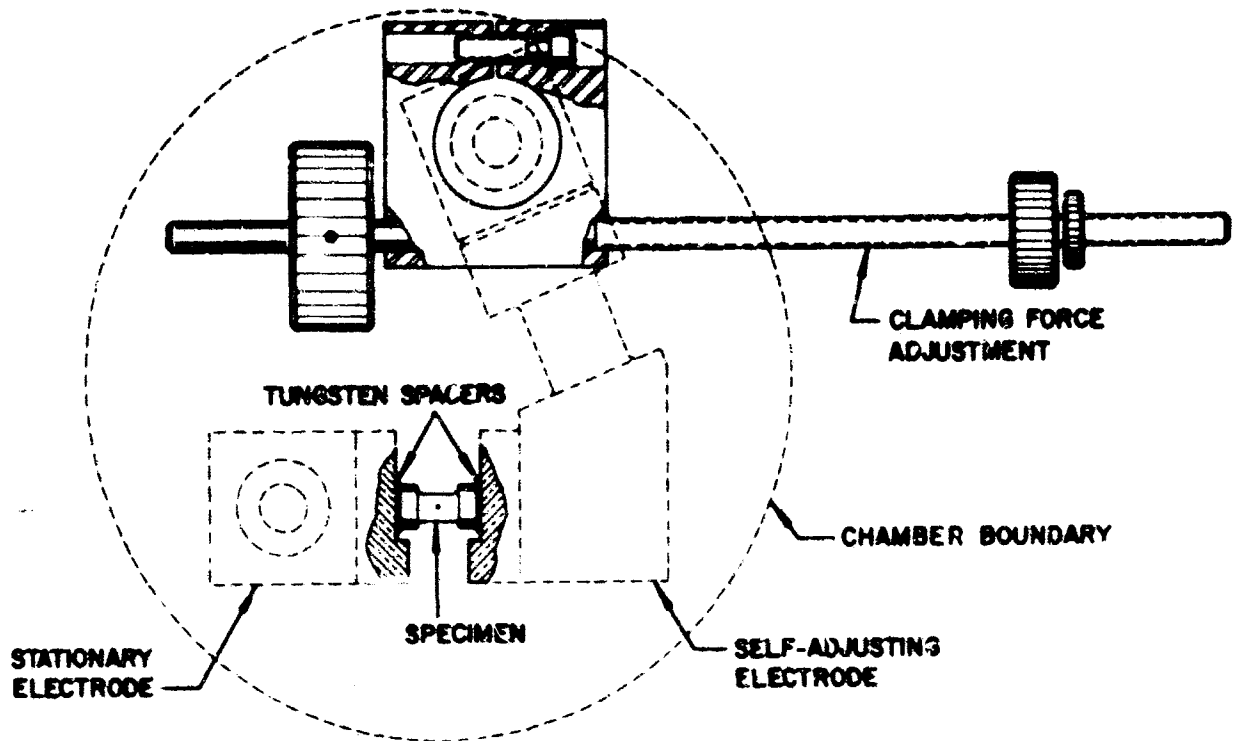


Figure 4. Face-to-Face Clamping of the Test Specimen, and Gravity Balance System.

of the furnace may cause brittle specimens to break; hence, the bearing assembly of the dynamic seal and power feedthrough (Figure 1) has been designed to eliminate any axial play of the feed-through shaft, while still maintaining the low friction required for precision adjustment of the clamping force.

B. POWER CONTROL

Power is supplied to the specimen by a 50 KVA step down transformer with secondary taps of 8, 12, and 15 volts. Power in the primary of the power transformer is derived from a full-wave silicon rectifier phase

control circuit. The gate trigger circuit for the phase control of the SCR's, which determines the average AC power delivered to the primary of the power transformer, comprises of a variable gain commercial magnetic amplifier-type trigger unit (Norbatrol Electronics, Pittsburgh, Pennsylvania), whose output in turn is controlled by the amount of DC current fed to its input terminals. The unit will deliver full power (45 KVA) at a DC input of 2 milliamperes.

The variable DC for controlling the trigger unit is obtained from a full wave rectifier circuit, which is fed by a variable AC from a DC motor-driven autotransformer. The speed of the DC drive is adjusted to the desired level by varying the field excitation current, while the direction of rotation is controlled by the polarity of power supplied to the armature windings. The power application rates can be varied between 20 and 15,000 watts per second, and are controlled by foot switches (FS₁, FS₂, and FS₃ in Figure 5) located at the operator's site. The relays shown in the circuit schematic in Figure 5 are used to activate the various controls, and are partially interlocked to prevent accidental operating mistakes.

Pressing the foot pedal FS₁, turns on coil M of the magnetic contactor, which connects the line power to the furnace. Foot switch FS₃ energizes relay HV, whose contacts are interconnected such, as to drive the DC motor counter-clockwise; voltage output of the variac and hence power to the furnace increases. Activation of foot switch FS₂ causes the motor to turn in the opposite direction, and power is lowered.

Power to the furnace is cut off by releasing the hold-down latch on foot switch FS₁, which turns off contactor coil B. A second pair of contacts on FS₁ which are closed in the "off" position of the switch, energize a relay (marked "off" in Figure 5) which causes the DC control current for the SCR trigger circuit to go down to zero. When the wiper of the autotransformer reaches the zero output position, the contacts of a limiting switch LLS open, disengage relay, "off" and thus turn off the power to the DC-drive.

Once the power has been turned off, relay M cannot be reenergized unless either the variac setting has reached its minimum position (contact LLS

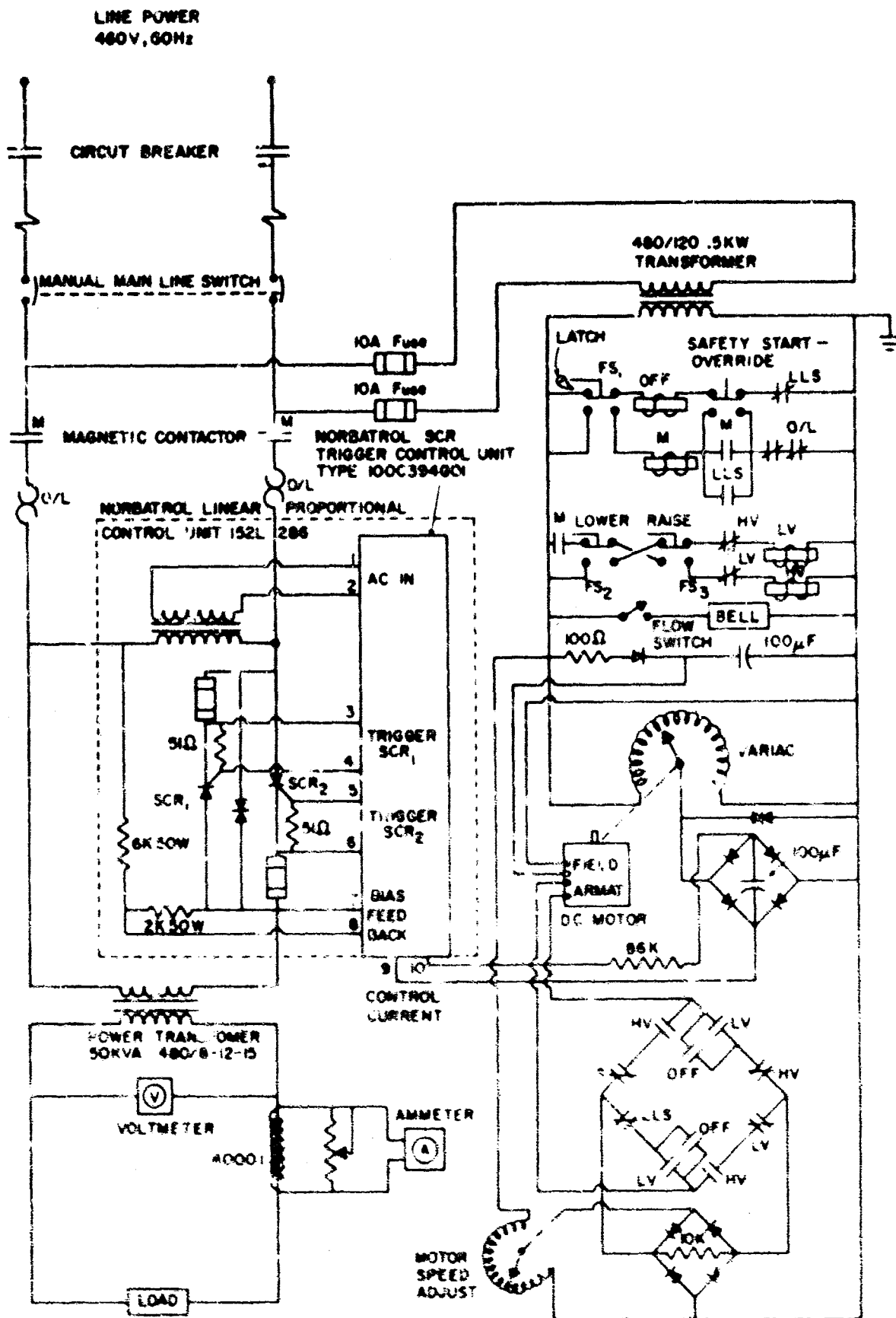


Figure 5. Power Supply and Control System for the Melting Point Furnace.

closed), or a separate switch (safety start-overrid.) switch in Figure 5) is pressed, which interrupts the down-drive of the variac and provides a bypass for the normally open contacts M and LLS in the current path of the coil M.

The entire power circuit is protected by main fuses (not shown in Figure 5), and by two bimetallic switches O/L, which disconnect the line power in case of thermal overload. The cooling water to the furnace is monitored by a flow-switch, which turns on a bell in case of insufficient water pressure, or failure to provide cooling water to the furnace.

C. OPERATION

After insertion of the specimen into the clamping device of the furnace and closing the furnace lid, the chamber is evacuated several times, and is each time refilled with high purity helium to ambient pressure. The specimen is then heated up and held for a few minutes under vacuum to allow eventual gas contaminants to escape. The melting point run can be made under vacuum, maintaining a slight gas bleed to avoid fogging of the quartz window; for very high temperature runs, however, where rapid vaporization may cause concentration shifts, the furnace is usually pressurized with high purity helium or argon to a maximum pressure of six atmospheres.

Presuming that the approximate melting ranges are known, the temperature of the specimen is brought rapidly to within approximately 50°C of the expected melting temperature. Then, in order to avoid loss of the specimen by accidental overshooting, the heating rate is lowered to allow stepwise power increases varying from approximately 2 to 10°C. A typical appearance of the center portion of a sample, photographed just before melting was noted, is shown in Figure 6.

Due to the steep temperature gradient, the formation of liquid first occurs in the interior, thus allowing the observer sufficient time to focus the pyrometer and to match the filament exactly against the radiation background from the black body hole.

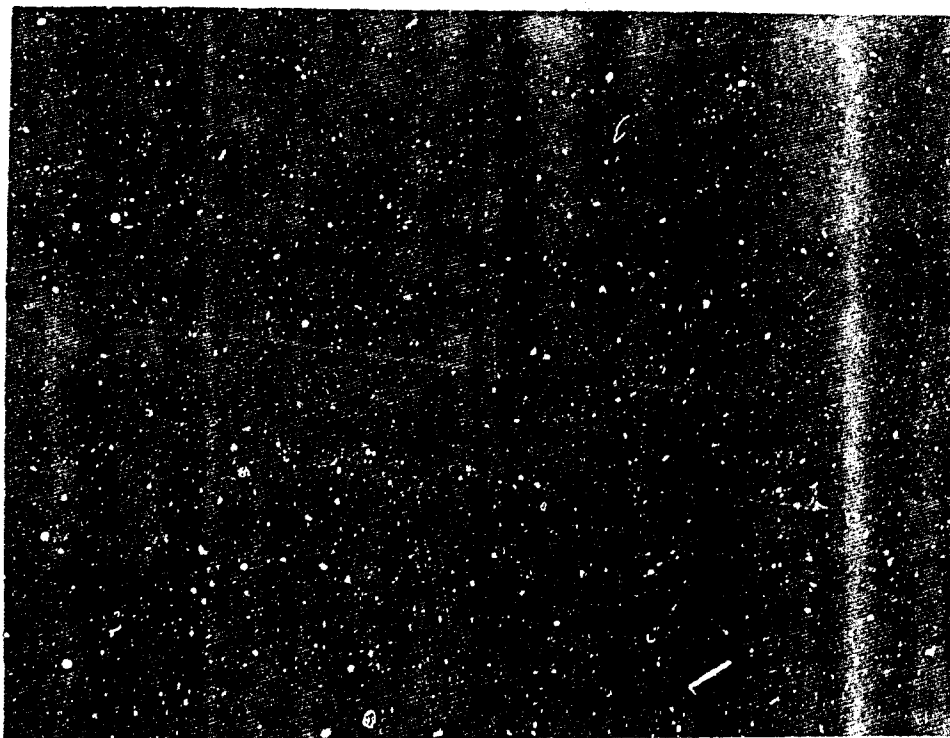


Figure 6. View Through the Observation Window at a Melting Point Specimen at Temperature. X8

The run is usually completed when the black body hole either fills with liquid (Figure 7), or the specimen collapses.

In general, it is found that porous specimens (20-40%) are preferable to fully dense material, as considerable less sputtering of the melt is encountered and the temperature readings can be performed more accurately. In dense specimens, the temperature interval between the formation of the first melt and the point where the hole fills with liquid, is very small; and the melt exuding from the interior tends to resolidify at the colder outer portions, causing the sample to burst upon further power increases. In porous specimens, however, the colder outer shell tends to soak up the melt from the interior, creating a cavity in the center portion (Figure 8). Slight power increases do not increase the temperature, but merely affect the amount of melt formed. Thus, a very pronounced temperature

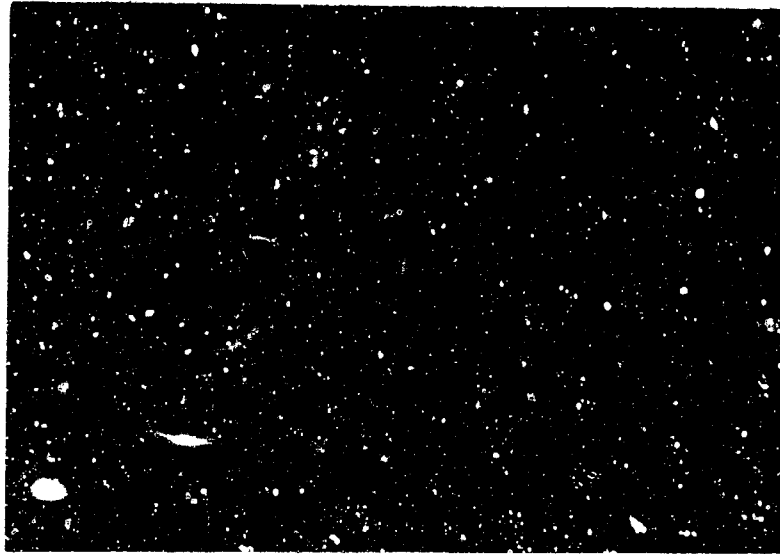


Figure 7. Typical Appearance of a Pirani Melting Point Specimen After Melting.
Note Black Body Hole Filled with Liquid.

X8

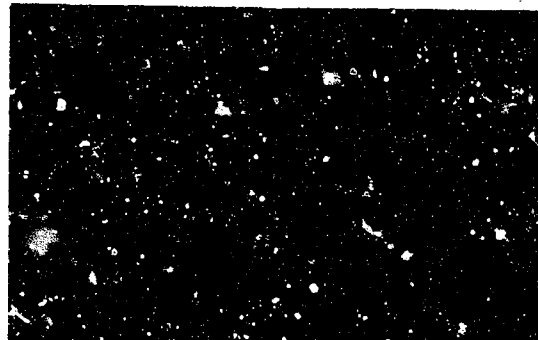
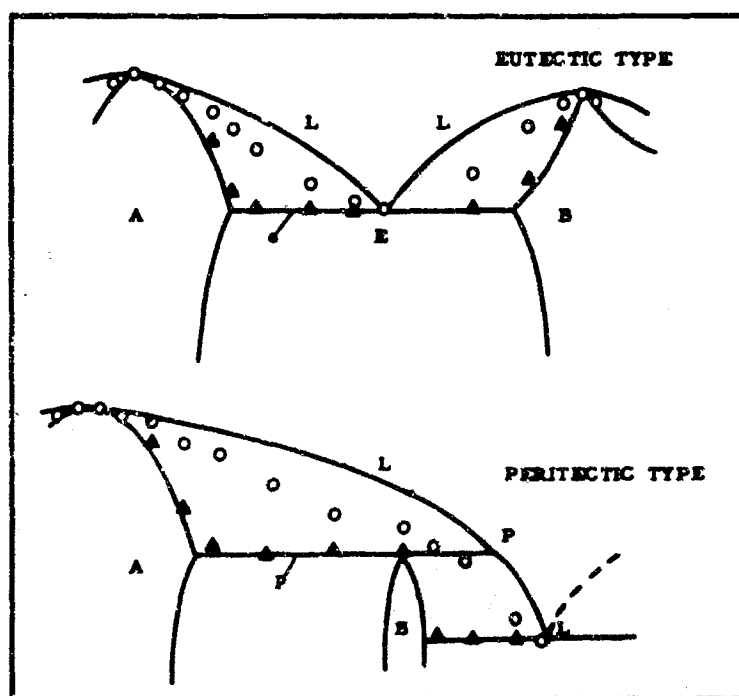


Figure 8. Sectioned Porous Melting Point Sample After Incipient Melting was Noted.

hold is produced, which serves as a useful additional indication for the temperature of the phase change. Upon further power increase, the boundaries of the melt-cavity ultimately reach the outer sample surface, and the specimen finally collapses.

In the measurements, the most precise data are obtained for isothermally melting alloys (eutectic and maximum melting compositions); in strongly two-phased melting alloys, i.e. alloys whose compositions are close to the homogeneity boundaries of higher melting phases, incipient melting is difficult to note, and the temperature data obtained tend to be high. After incipient melting, the specimens usually start to sag, and, finally, the black body hole gradually closes before the liquidus boundary has been reached. Typical melting patterns for a eutectic and a peritectic case as obtained with the Pirani technique are shown in Figure 9. It will be noticed, that at



- A, B Intermediate Phases
- L Liquidus Lines
- e, P Eutectic and Peritectic Line
- E, P Composition of the Eutectic and the Peritectic
- ▲ Incipient Melting Observed
- Sample Collapses Due to Loss in Strength

Figure 9. Typical Melting Behavior Observed with the Pirani-Technique.

concentrations approaching the locations of melting point maxima as well as those of eutectica, the difference between observed incipient melting temperature and the temperature, at which the sample collapses, narrows; both temperatures, of course, coincide when these respective concentration points are reached. The differentiation between peritectic and eutectic reaction types can usually be achieved without difficulty from an analysis of the melting pattern (Figure 9).

IV. TEMPERATURE MEASUREMENT

In all the measurements performed so far, micro-optical pyrometers manufactured by the Pyrometer Instrument Co., Inc., Bergenfield, New Jersey, have been used. These pyrometers have three overlapping black body scales on direct reading milliammeters; the ranges on the standard model are 700 - 1400°C, 1300 - 1900°C, and 1800 - 3200 (4500)°C, and the temperatures are measured at an effective wave length of 0.65 μ .

In the following sections, calibration of these pyrometers, as well as the procedures used to determine the temperature corrections for non-black body conditions at the sample and the losses in the observation window, will be discussed. A list of useful secondary temperature standards is also given.

A. PYROMETER CALIBRATION

Two separate procedures are involved in the calibration of the pyrometers: Calibration of the pyrometer proper, and calibration and adjustment of the meter readout for the filament current.

The objective of the calibration of the pyrometer is to establish a precise relationship between filament current and temperature, using calibrated radiation sources or pyrometers as standards. For temperatures up to 2300°C, the pyrometer is either compared with standard pyrometers certified by the National Bureau of Standards, or against a certified tungsten ribbon-filament lamp with precisely known current-temperature relationship.

For calibration points at higher temperatures, the carbon-arc technique^(2, 29, 30), using an arc-furnace manufactured from the Mole-Richardson Company, Hollywood, California, was employed. Based on data from the National Bureau of Standards⁽³¹⁾ a temperature of $3808^{\circ} \pm 20^{\circ}\text{K}$ was asserted to the crater of the anode, when operated in the region of the quiet arc. Lower temperature fixed points were obtained in the well-known manner using absorbing glasses of accurately known transmission.

In the calibration runs, at least five readings were taken at each point. The current through the pyrometer filament is determined by the voltage drop across a 10Ω precision (5 ppm) resistor, and recorded to the nearest one or ten microamps. A current temperature-filament current relationship is then established by a least square fit of the data.

The same meter and resistor are employed to calibrate the temperature scale of the milliammeter provided with the pyrometer. The calibration is usually started at the low temperature end and at least five readings are taken at each of the selected cardinal points; after averaging, the meter reading is then adjusted to comply with the established pyrometer-filament current relationship.

The total temperature error is composed of several parts: The uncertainties in the calibration equipment and the individual calibration steps.

Considering the first error sources first, the data given in Table 1 represent the uncertainty levels assigned to the certified pyrometers. Although the data probably correspond more to estimates rather than presenting exact values, the data are claimed to have a confidence level of more than 95%⁽³¹⁾.

Typical uncertainties introduced by the visual matching of test and calibration pyrometers are $\pm 1.7^{\circ}\text{C}$, and hysteresis effects in the micro-optical pyrometers in use at this laboratory amount to approximately 1.8°C ;

Table 1. Temperature Uncertainties in the NBS Certified Standard Pyrometers and Tungsten Ribbon-Filament Lamps⁽³¹⁾, (95% Confidence Level)

	<u>Temperature °C</u>	<u>Uncertainty °C</u>
<u>Certified Pyrometer:</u>	800	± 4
	1063	± 3
	2800	± 8
	4000	± 40 max.
<u>Tungsten Ribbon Lamp:</u>	800	± 5
	1100	± 3
	2300	± 7

a further uncertainty of approximately $\pm 3^\circ\text{C}$ maximum at high temperature end is introduced by the limited resolution of the ten-turn pot used in the pyrometer. A least square fit of the calibration data, and incorporating the uncertainties of the temperature standards, yielded the error limits listed in Table 2.

Table 2. Overall Temperature Uncertainties for the Micro-Optical Pyrometers.

<u>Temperature °C</u>	<u>Uncertainty ± °C</u>
1100	4
2000	7
2300	8
3600	10
3600	25

B. CORRECTION TERMS FOR NON-BLACK BODY CONDITIONS OF THE HOLE AND FOR LOSSES IN THE QUARTZ WINDOW

In the experimental work, usually a wide variety of different materials is encountered in experiments, for most of which the emissivity coefficients are unknown. Furthermore, the emissivities of a given material are strongly dependent upon its surface conditions; hence, to eliminate as effectively as possible variations of the apparent temperatures, the conditions, under which the measurements are to be made, must resemble closely those of a true black body, regardless of the type and surface condition of the test material.

To determine the average effect of hole geometry upon the apparent emissivity, a variety of different materials, including specimens of tungsten, tantalum, molybdenum, as well as of refractory compounds such as TaC, HfC, TaB₂, and HfB₂, was fabricated into cylindrical shapes and provided with holes of varying diameter to depth ratios. All samples comprised of compacts which were sintered from 60 μ average powder stock and showed varying degrees of surface roughness.

The apparent emissivity coefficients were determined from the apparent temperatures of the sample holes, as compared to that of a true black body source, for which a 0.5 mm dia x 10 mm deep hole drilled into the graphite sample holder served as the standard.

Since for all cases investigated, ϵ was above .95, the simplified equation (1) was used for the calculation of the emissivity coefficients:

$$T_s - T_{gr} = -T_s^2 \cdot \frac{C_2}{\lambda} \ln \epsilon, \quad (1)$$

where T_s denotes the apparent temperature of the sample black body hole, T_{gr} the temperature of the radiating cavity in graphite, C_2 (Planck's second radiation constant) = $\frac{hc}{k} = \text{const} = 1.4384$ [cm.grad.], λ the effective wavelength used in the measurements (0.65 μ), and ϵ stands for the emissivity coefficient.

The observed emissivities, as calculated from equation (1), were found to be only slightly dependent upon the test material, but are significantly affected by the geometry of the black body hole, as evidenced from the data compiled in Table 3.

Table 3. Mean Emissivity Coefficient of Black Body Holes in Metallic Specimens (Rough Surface).

<u>Hole Dimensions (dia x depth, mm)</u>	<u>Mean Emissivity Coefficient</u>
1.3 x 3	0.97
1.0 x 3	0.98
0.6 x 3	0.995

The temperature correction terms, as computed from equation (1) for the interesting range of emissivity factors, are shown in graphical form in Figure 10.

The losses in the quartz windows arise from two mechanisms: Reflection at the two surfaces, and absorption of radiant energy within the quartz plate.

The absorption of quartz at 0.65μ , the wavelength used in the pyrometer, is small; under these conditions, the total transmission, T_{tr} , of the quartz window is given to a sufficient degree of accuracy by

$$T_{tr} = D \cdot A$$

D.....Relative reflection loss at the surfaces of the quartz window

A.....Relative absorption loss in the quartz window

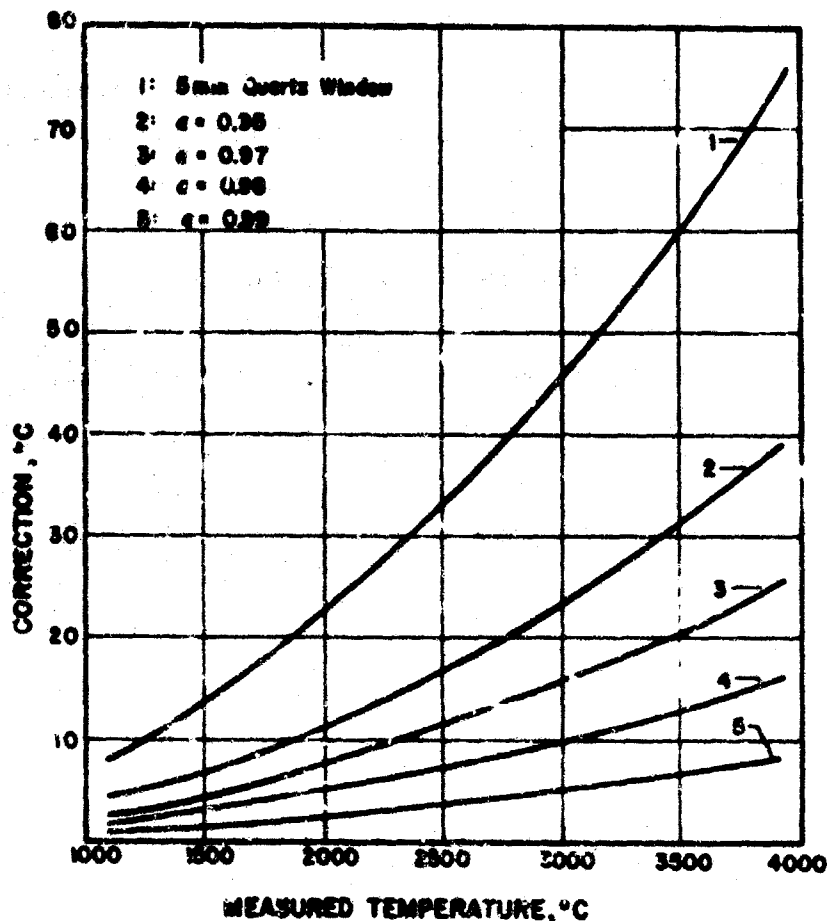


Figure 10. Temperature Correction Chart for the Pirani Furnace.

The terms D and A can be calculated separately from the known absorption data and the refractive index for quartz for the particular wavelength. For the brand used (GE-grade 101, $d = 5$ mm), $n = 1.4585$. From Fresnel's formula for vertical incidence,

$$D = \frac{T_r}{T_o} = \left(\frac{n-1}{n+1} \right)^2 \quad (2)$$

a reflection loss of $D = 3.48\%$ per surface is calculated. Together with a transparency coefficient of 0.98 per cm at $\lambda = 0.65\mu$, a total transmission of $T_{tr} = D \cdot A = 0.92$ is obtained for the quartz window.

An experimental check of the value was performed using the following considerations:

The amount of energy radiated within a wavelength interval λ and $\lambda + d\lambda$ by one square centimeter of surface area having the temperature T is given by

$$E(\lambda, T) = T(\lambda) \cdot e(\lambda, T), \quad (3)$$

where $\epsilon(\lambda, T)$ denotes the emissivity coefficient of the radiating surface, and $e(\lambda, T)$ is Planck's function

$$e(\lambda, T) = \frac{c^2 \cdot h}{\lambda^5} \cdot \frac{1}{\frac{h\nu}{k\lambda \cdot T} - 1} \quad (4)$$

If the radiation passes through a medium having a transmittance $T(\lambda)$, the amount of radiant energy leaving the system is given by

$$E_1(\lambda, T) = T(\lambda) \cdot \epsilon(\lambda, T) \cdot e(\lambda, T) \quad (5)$$

$E_1(\lambda, T)$ is converted by the pyrometer into an apparent black-body temperature T_m according to

$$E_1(\lambda, T_m) = e(\lambda, T_m) \quad (6)$$

In order to find the true temperature of the radiating surface, we have to equate $E_1(\lambda, T)$ with $E_1(\lambda, T_m)$, i.e. we ask for the temperature, which a radiant surface of $\epsilon = \epsilon(\lambda, T)$ must have, in order to deliver through a system with a total transmission T_{tr} the same amount of radiation as a black body at the temperature T_m .

Hence,

$$\frac{T_{tr}(\lambda, T)}{C_2} = \frac{1}{C_2} \quad (7)$$

$$e^{-\frac{C_2}{\lambda \cdot T} - 1} = e^{-\frac{C_2}{\lambda \cdot T_m} - 1}$$

For temperatures below 4500°K and a wavelength of 0.65μ, $\lambda T \ll C_2$ (region where Wien's law applies); under this condition, equation (7) reduces to

$$A \cdot e^{-\frac{C_2}{\lambda \cdot T}} = e^{-\frac{C_2}{\lambda \cdot T_m}}$$

or

$$\ln A = -\frac{C_2}{\lambda} \cdot \frac{T - T_m}{T \cdot T_m} \quad (3)$$

For the case, that $A(\lambda, T)$ does not deviate too much from unity, we may set $T \cdot T_m \approx T_m^2$, and obtain for the temperature correction term

$$T_{true} - T_m = \Delta T = -T_m^2 \frac{\lambda}{C_2} \ln A \quad (9)$$

Provided that n is not too large, the total transmission of a system of n equal quartz windows is given by

$$T_{tot}(n) = (D \cdot A)^n \quad (10)$$

Making use of formula (9), we find the incremental temperature correction per quartz window practically constant, and equal to

$$\Delta T (n = 1) = -T_m^2 \cdot \frac{\lambda}{C_2} \ln D \cdot A$$

Thus, by measuring the apparent temperature of a radiation source through a varying number of quartz windows, the term $D \cdot A$ can be evaluated independently from the value of ϵ .

Experiments were performed using 1, 2, and 3 quartz windows. As reference point for the measurements served a 0.5 mm dia. and 10 mm deep hole in graphite, as described further above. At 2245°C, the chosen equilibrium temperature, the following data were obtained (Table 4).

Table 4. Effect of the Number of Quartz Windows ($d = 5$ mm) Upon the Apparent Temperatures of a Black Body Source

Number of Quartz Windows	Measured Temp. °C	Difference (Mean Value)
1	2245 \pm 4	-
2	2220 \pm 4	25
3	2193 \pm 4	26

The mean incremental temperature difference per quartz window, derived from a large number of readings was 25.5°C, yielding, in good agreement with the theoretical value, a product of $D \cdot A = 0.915$ (formula 9). The corresponding corrections for the quartz window, which are practically entirely due to reflection losses, are included in the chart shown in Figure 10.

Based on these data, the hole dimensions used in the experimental samples have been standardized to dimensions of 0.6 mm diameter, and a minimum depth of 4 mm, leaving only a negligible correction for non-black body conditions (Figure 10).

C. SECONDARY TEMPERATURE STANDARDS

In the course of experimental work, it is often desirable to be able to quickly check the status of calibration of the pyrometer, to test the consistency of calibration among a set of temperature measuring instruments, and also to compare and eliminate errors due to individual reading habits of laboratory personnel carrying out the experiments. Furthermore, accurately known and easily reproducible melting points of proper alloy combinations can be used directly as calibration standards.

Accurate fixed points presently in use as secondary temperature standards are based on the melting points of certain metals. They are listed in Table 5.

Table 5. Fixed Temperature Points (New International Scale, 1949)

Metal	Freezing Point
gold	1063°C
nickel	1453°C
palladium	1552°C
platinum	1769°C

As has been discussed by W. Hume-Rothery⁽⁴⁾, et al., the main problem in using the melting points of elements as temperature standards is the danger of contaminants, which may change significantly the freezing point; furthermore, metals, where contamination is less of a problem, are usually prohibitively expensive for every-day purposes.

No officially accepted secondary fixed points have been established as of yet for temperatures above the freezing point of platinum, although a large number of fairly consistent melting point values on refractory metals has been reported.

In the course of work on refractory alloy systems in this laboratory, which mainly involved metal-carbon and metal-boron combinations, it was found, that the temperature of certain binary and pseudobinary eutectics could be reproduced with a fairly high degree of accuracy, and control of the impurity levels to within the limits, where noticeable changes would occur, could be maintained with ease.

Among the combinations listed in Table 6, those involving the carbides are probably the most useful: The samples can be contained in graphite crucibles, fabricable from commercially available graphite grades, and the measurements can be carried out in graphite-element furnaces, at hand in almost every laboratory working in the refractory materials field. The need for specialized and expensive equipment is thus eliminated.

So far, the largest number of measurements have been carried out on the eutectic equilibria existing between W and W_2C (22 At%, 2710°C) and between Mo and Mo_2C (17 At%, 2200°C); the corresponding temperatures may be therefore regarded as the most firmly established. In view of the simplicity of their preparation, and their insensitivity towards contamination, both combinations are extensively used in this laboratory as secondary temperature reference points in pyrometric temperature measurements, as well as for the determination of the overall transmissions of optical systems and the calibration of opto-electric temperature transducer systems.

In addition to the fixed points involving solid-liquid reactions (Table 6), two solid state reactions, namely the eutectoid decomposition of the cubic high temperature phases in the systems W-C and Mo-C (Table 7), also show excellent reproducibility and may serve as useful standards for calibrating and testing the sensitivity of the temperature transducer system in high temperature thermal analytic equipment.

Table 6. Secondary High Temperature Reference Points Based on Eutectic Reactions

System	Composition of Eutectic	Eutectic Phases	Accepted Temperatures, °C		
			Mean	Reproducibility	Estimated Overall Uncertainty
Mo-B	23 At.% B	Mo + Mo ₂ B	2175°	± 6°	± 10°
Mo-C	17 At.% C	Mo + Mo ₂ C	2200°	± 2°	± 8°
Nb-C	10.5 At.% C	Nb + Nb ₂ C	2353°	± 6°	± 10°
W-B	27 At.% B	W + W ₂ B	2600°	± 8°	± 12°
V-C	49.5 At.% B	VC + C	2625°	± 5°	± 10°
W-C	22 At.% C	W + W ₂ C	2710°	± 3°	± 10°
Ti-C	63 At.% C	TiC + C	2776°	± 6°	± 12°
Ta-C	12 At.% C	Ta + Ta ₂ C	2843°	± 10°	± 13°
Zr-C	64.5 At.% C	ZrC + C	2911°	± 12°	± 18°
Hf-C	65 At.% C	HfC + C	3180°	± 20°	± 30°
Nb-C	60 At.% C	NbC + C	3305°	± 12°	± 20°
Ta-C	61 At.% C	TaC + C	3445°	± 5°	± 26°

Table 7. Secondary Temperature Standards, Based on Solid State Reactions

System	Composition of Eutectoid, At% C	Reaction*	Accepted Temperatures, °C		
			Mean	Reproducibility	Estimated Overall Uncertainty
Mo-C	39	$\alpha\text{-MoC}_{1-x} \rightleftharpoons \eta\text{-MoC}_{1-x} + \text{C}$	1960	± 10°	± 15°
W-C	37.5	$\alpha\text{-WC}_{1-x} \rightleftharpoons \beta\text{-W}_2\text{C} + \text{C}$	2530	± 15°	± 20°

* The reactions in both systems are fast, and no significant temperature shifts will be noticed at heating or cooling rates below 10°C per second.

V. PREPARATION OF TEST SPECIMENS

All three major techniques used in refractory materials processing, namely cold-pressing and sintering, hot-pressing, and melting, are employed in the preparation.

Where it can be tolerated, hot pressing is no doubt the most expedient of all methods in obtaining compact and strong samples; however, application of this method is restricted by the interaction of the test material with the die components. Subjected to a lesser degree to contamination, and hence more versatile in its application, is the cold pressing and sintering technique. A disadvantage of this method is the addition of a second processing step and the requirement for expensive high temperature sintering furnaces to achieve sufficient densification of the samples, so they can be handled without danger of breakage. The third method, melting of the alloys in an arc or electron beam furnace, and subsequent machining of the ingots into the required dimensions, is undoubtedly the slowest and most expensive of the methods discussed, but is sometimes employed to prepare alloys from components not available in powder form, or to remove volatile impurities (cf. oxygen, nitrogen, volatile oxides) from contaminated stock.

Bar-shaped specimens of carbides, for example, can be hot pressed on one step to final shape in the split die assembly shown in Figure 11. Usually, however, the powder mixtures are first hot pressed to yield elongated cylinders of 10 to 15 mm in diameter, which then are ground to shape and provided with a black body hole (Figure 12).

Ductile metal specimens, or samples containing an excess amount of ductile phases, are pressed to final shape (with 0.6 mm dia. and 4 mm deep hole) in a split die assembly with retractable center pin (Figure 13) and are used in the as-pressed state (Figure 14). Samples of more brittle materials are sintered after cold-pressing to acquire sufficient strength to be handled in the melting point furnace.



Figure 11. Graphite Die and Heater Components for Hot Pressing Bar-Shaped Melting Point Specimens

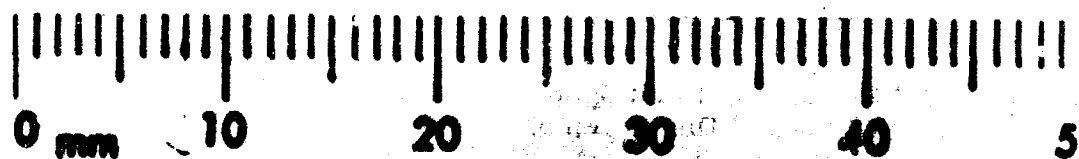


Figure 12. Pirani Melting Point Specimen, Hot Pressed and Ground to Shape.

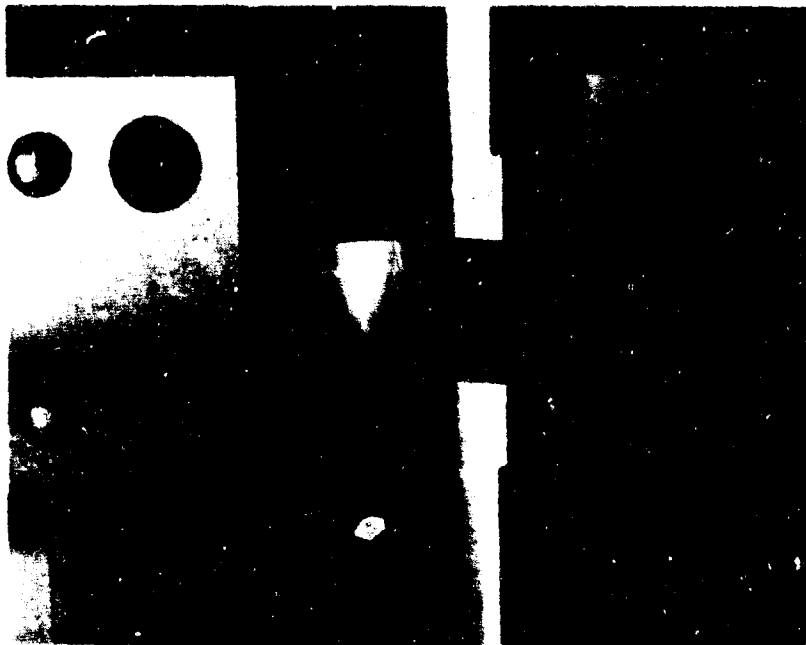


Figure 13. Shaped Die with Retractable Center Pin for Cold Pressing Melting Point Specimens. (Front Half of Die Removed)



Figure 14. Melting Point Specimen, Cold Pressed in the Shaped Die Assembly Shown in Figure 13.

VI. MEASUREMENTS

Over the past two years, numerous measurements on refractory alloys have been carried out with the Pirani furnace which have resulted in a number of revisions to the existing literature data. Their complete presentation, however, would exceed the scope of this report. Hence, only a selection of data on refractory metals and selected binary alloys and compounds of the refractory transition metals are presented, where existing literature data allow a comparison of the test results. For a comprehensive description of the carbide solutions, reference is made to a report series, AFML-TR-65-2, issued during the past two years⁽³²⁾.

A. MELTING POINTS OF REFRACTORY METALS

The melting temperatures measured for various refractory metals, together with data found in the literature, are presented in Table 8.

The titanium used in our measurements consisted of samples which were machined from electron-beam molten iodide-titanium stock. Total impurities as determined by chemical and spectrographic analysis after melting was less than 250 ppm; of these impurities, * 150 ppm were estimated to be oxygen, nitrogen, and carbon. The α - β -transformation temperature of 887°C in the processed and melted material, determined by differential thermal analysis, was the same as in the iodide titanium; since even small amounts of oxygen have a pronounced effect upon the transition temperature, this result indicates that practically no contamination by interstitial elements had taken place during the melting point runs.

The zirconium samples comprised of cold-pressed and high vacuum sintered bars, which were prepared from commercial zirconium powder and from high-purity crystal bar zirconium. Major impurities in the zirconium powder were (contents in ppm): C-40,

*Oxygen was hot-extracted in a gas-fusion analyzer using a platinum bath at 2300°C.

Table 8: Melting Points of Refractory Metals

Metal	Literature Values, °C	Number of Measurements	This Investigation (Values in °C)		
			Mean Value	Standard** Deviation	Accuracy*
Ti	1672 ± 4° (34) 1676 ± 10° (35) 1660° (36)	8	1668°	± 8°	± 4°
Zr	1868 ± 10° (34) 1855 ± 15° (37)	5	1876°	± 8°	± 4°
Hf	2230 ± 50° (38) 2222 ± 30° (37)	8	2218°	± 10°	± 6°
V	1919 ± 2° (34) 1900 ± 24° (39) 1888 ± 10° (40)	4	1926°	± 6°	± 3°
Nb	2585° (41) 2430° (28) 2468 ± 10° 2497° (39)	6	2475°	± 10°	± 4°
Ta	3006 ± 15° (43) 3000° (44) 2997° (39)	6	3014°	± 14°	± 10°
Mo	2618 ± 3° (43) 2630 ± 50° (45)	9	2619°	± 9°	± 4°
W	3380 (25) 3410 ± 15° (45) 3417° (2)	3	3423°	± 26°	± 10°
Re	3140 ± 20 (24) 3160° (48) 3170° (46) 3170 ± 60° (49) 3180° (47) 3180 ± 20° (50)	8	3075°	± 14°	± 7°

* Standard Deviation in the Measurements
 ** Including Errors in the Pyrometer Calibration

Fe -315, Hf-67, O-830, Ta-<200, sum of other impurities-<460. The total impurity content in the crystal-bar zirconium was below 300 ppm. Both materials yielded within the error limits of the same melting temperature (Table 8).

The analysis of the hafnium sponge, from which the melting point specimens were prepared by electron-beam melting and machining, was as follows (impurities in ppm): Al-20, C 210, Nb-680, Cr-<20, Cu-40, Fe-265, H-55, Mo-40, N-200, O-810, Si-<40, Ta-<200, Ti-20, W-235, sum of remainder-<100. After electron beam melting, the combined oxygen and nitrogen content was below 300 ppm. The zirconium content of the product was 1.9 atomic percent.

To achieve better desoxidizing conditions, one atomic percent boron was added to another hafnium batch prior to melting and the resulting bars also fabricated into test specimens. A third test series was run on cold-pressed and high vacuum sintered specimens, which were prepared from hafnium powder having similar impurity contents as the hafnium sponge. No substantial fluctuation in the melting point data could be observed, suggesting, that the impurity levels were low enough as not to have any noticeable effect upon the melting points.

The analysis of the group V metals is given in Table 9. The specimens were prepared by cold-pressing, cold-pressing and sintering, as well as by electron-beam melting technique in order to remove volatile impurities. The test data are compiled in Table 8.

While little effect of slight impurity differences upon the observed melting point was noticed for vanadium and niobium, a drop from 3014°C, for a tantalum with less than 200 ppm O + N + Fe + Si, to 2960°C, for samples which contained approximately 60 ppm oxygen and nitrogen and 300 ppm of other materials, was observed⁽³³⁾.

The molybdenum and tungsten specimens were prepared from powders having a purity better than 99.9 percent. To achieve

Table 9. Chemical Analysis of the Group V Metal Powders

Impurity	Vanadium	Niobium	Tantalum
N	340	68	50
O	650	380	280
C	300	110	140
Ta	n. d.	500	-
W	-	1150	-
Zr	n. d.	250	-
Nb	n. i.	-	100
Si	80	<10	<30
Sum of other metallic impurities	300	<500	<300

sufficient strength, the powder compacts were presintered for 2 hours at 1600°C under high vacuum (4×10^{-6} Torr).

Major contaminants determined in the processed specimens were: In molybdenum: O-88 ppm, Si-60 ppm, W-200 ppm; in tungsten: Fe-20 ppm, N-20 ppm, O-110 ppm, and Mo-50 ppm. The rhenium powder had the following impurity levels (in ppm): Fe-23, Al-<1, Ni-<1, Si-<1, sum of other impurities-<10.

In general, our data obtained for the refractory metals are in good agreement with values given earlier in the literature (Table 8). The only large discrepancy, our value being approximately 100°C than the previously accepted melting point of 3160°C, was obtained for rhenium. A comparison of the impurity levels in our material as compared to the product used by previous investigators does not suggest the possibility of contamination as being responsible for the observed difference. Also, the data obtained on a second sample series, which was prepared by electron-beam melting the presintered bars, reproduced within 7°C the results

obtained on the cold-pressed and sintered samples. The close agreement between the data of at least five independent investigators appears therefore as surprising; an independent contest of the melting data on rhenium apparently is needed.

B. SOLIDUS TEMPERATURES OF REFRACTORY METAL-CARBON ALLOYS

Among the known alloys, the monocarbides of the refractory transition metals are the highest melting compounds in existence. With the exception of chromium, all of the elements of the group IV to group VI elements form congruent melting carbides in the vicinity of the equiatomic concentration region. In neither instance, however, does maximum melting occur at the stoichiometric composition, but appears to be shifted to lower carbon concentrations. The group IV and group V metal monocarbides are characterized by a wide range of defect solid solutions, and, with the exception of TaC, for which a rather steep concentration dependence was noted⁽³³⁾, the phases melt with rather flat maxima. The occurrence of the cubic phases in the group VI metal carbon system is restricted to the concentration range around 40 atomic percent, i.e. they are stable at defect compositions only.

Table 10 lists the congruent melting temperatures of the cubic (B1) monocarbides. The data presented are based on a large number of measurements, which were carried out on high purity and analytically defined material in the course of reinvestigations of the binary metal-carbon systems⁽³²⁾. The maximum solidus temperatures of the Me_3C phases, and of Cr_3C_2 are listed in Table 11, while data for the eutectic reaction isotherms for metal + metal carbide, and monocarbide + graphite, are presented in Tables 12 and 13.

C. SOLIDUS TEMPERATURES OF REFRACTORY METAL-BORON ALLOYS

Compared to the refractory carbides, very few reliable melting points are available for alloys of the refractory transition metals with boron. Oxygen contamination of the starting material is the

Table 10. Congruent Melting Points of Cubic (B1) Refractory Monocarbides.

Carbide	Literature Values °C	This Investigation, °C		
		T_f	Comps. At. % C	Average Reproducibility
TiC	5160 ± 100° (52) 3250° (55) 3140° (53) 2940° (56) 3030° (54)	3067 ± 25°	44 ± 1	± 15°
ZrC	3532 ± 125° (2) 3535° (59) 3400 ± 50 (ZrC _{0.92}) (57) 3420° (ZrC _{0.93}) (8, 58)	3440 ± 25°	45 ± 1	± 10°
HfC*	3887 ± 150° (2) 3830 (HfC _{0.99}) (9, 61) 3895 (HfC _{0.98}) (22) 3820 ± 100° (HfC _{0.96}) (60)	3978 ± 40°	48.5 ± 0.3	± 20°
VC	2750° (62) 2650°C (peritect. dec) (40) 2830° (52) 2789° (56)	2648 ± 12°	43 ± 0.5	± 8°
NbC	3490 (59) 3600 ± 50° (23) 3500 ± 75° (NbC _{0.90}) (48) 3420° (NbC _{0.92}) (56)	2613 ± 26°	44 ± 1	± 8°
TaC	3875 ± 150° (2) 3540° (64) 4000-4200 (63) 3780° (59) 3825° (52) 3740° (24)	3983 ± 40°	47 ± 0.5	± 15°
α-MoC _{1-x}	2692 ± 50° (MoC) (2) 2700° (7) 2570° (MoC) (52) 2650° (32) 2870° (56)	2600 ± 10°	42 ± 1	± 5°
β-MoC _{1-x}	2785° (peritect. dec. at WC _{1.0}) (65, 66)	2747 ± 12°	39 ± 1	± 8°

* Mean Value and Estimated Overall Temperature Uncertainty.

Table 11. Maximum Solidus Temperatures of Selected Carbide Phases (Temperatures in °C)

Carbide	Literature Values	This Investigation, °C			Remarks
		T _{solidus} [*]	Comp [*] At% C	Average Reproducibility	
V ₂ C	2165 + 25° (40) 1850°C (67)	2187 ± 10°	35 ± 0.5	+ 8°	Peritectic decomp.
Nb ₂ C	3090° (28) 3080 ± 50° (23, 68)	2035 ± 20°	~ 35	± 15°	Peritectic decomp.
Ta ₂ C	3400° (19) 3500°C (68) 3240°C (61)	3330 ± 30°	~35.5	± 8°	Peritectic decomp.
Cr ₃ C ₂	1895° (70) 1830° (73) 1850° (71)	1831 ± 3°	~40	± 6°	Peritectic decomp.
Mo ₂ C	2400°C (65) 230-2330° (52) 2690 + 50° (2) 2410°C (69, 73) 2440 ± 30° (74)	2522 ± 10°	34.0 ± 0.5	± 5°	Congruent melting
η-MoC _{1-x}	-	2550 ± 10°	39.0 ± 0.5	± 5°	Congruent melting
W ₂ C	2857 ± 50° (4) 2860° (75) 2730 ± 15° (76) 2750 ± 50° (77) 2795°C (30 At.% C) (65, 66)	2776 ± 14°	31 ± 0.5	± 7°	Congruent melting
W ₃ C	2667 ± 50° (2) 2650 ± 50° (78) 2720° (68) 2780°C (75) 2755° (65, 66)	2770 ± 10	50 ± 0.3	± 4°	Peritectic decomp.

* Mean value and estimated overall temperature uncertainty

Table 12. Metal + Metal Carbide Eutectic Reaction Isotherms

Eutectic Constituents	Literature Values, °C	This Investigation, °C		
		T _{eut.} *	Eutect. Compos. At. % C	Average Reproducibility
β-Ti + TiC	1645 ± 8° (18) 1750° (peritect. dec.) (79)	1650 ± 7°	1.5 ± 0.5	± 3°
β-Zr + ZrC	1850° (*, 58) 1810° (57) 1830° (80)	1835 ± 20°	3 ± 1.5	± 15°
β-Hf + α-(HfC)-ss	- -	2180 ± 12°	1.5 ± 0.7	± 10°
V + V ₂ C	1630 ± 20° (17 At% C) (46) 1650° (67)	1650 ± 7°	15 ± 1	± 6°
Nb + Nb ₂ C	2335° (29, 81) 2330° (82) 2328° (68) 2340 ± 20° (13.5 At% C) (23)	2553 ± 10°	10.5 ± 0.5	± 6°
Ta + Ta ₂ C	2800° (11 At% C) (69) 2902 ± 30° (68) 2825° (12.5 At% C) (70)	2843 ± 15°	12 ± 0.5	± 7°
Mo + Mo ₂ C	2200° (7, 68)	2200 ± 8°	17 ± 1.5	± 2°
W + W ₂ C	2690° (18 At% C) (78) 2475° (19 At% C) (77) 2732° (68) 2710° (25 At% C) (65, 66)	2710 ± 10°	24 ± 1	± 3°

* Mean Value and Estimated Overall Temperature Uncertainty

Table 13. Metal Carbide + Graphite Eutectic Reaction Isotherms

Eutectic Constituents	Literature Values, °C	This Investigation, °C		
		T _{eutect.} *	Eutect. Compos. At. % C	Accuracy
TiC + C	3080° (83) 2780 ± 25° (84)	2776 ± 12°	63 ± 1.0	± 6°
ZrC + C	2850° (8, 51, 58) 2870 ± 30° (74) 2920 ± 50° (83)	2911 ± 19°	64.5 ± 1	± 12
HfC + C	3250° (83) 3400° (60) 2800° (85) 3220° (22) 2915° (86) 3150° (61, 9)	3180 ± 30°	65 ± 1	± 20°
VC + C	2830° (52) 2780° (56) 2750° (62) 2650° (peritect. isotherm)(40)	2625 ± 12°	49.5 ± 0.5	± 6°
NbC + C	3300 ± 50° (23) 3150° (83) 3220° (58) 3250° (28, 12)	3305 ± 20°	62 ± 4	± 12°
TaC + C	3710° (68) 3375° (61) 3310 ± 50° (83) 3300° (69)	3445 ± 26°	61 ± 0.5	± 5°
α-MoC _{1-x} + C	2470° (87) 2575° (74)	2584 ± 10°	45 ± 1.5	± 5°

* Mean Value and Estimated Overall Temperature Uncertainty.

common source of errors in transition metal alloys with carbon and nitrogen, is less harmful in this system class. With the exception of some lower-melting metal-rich eutectics, desoxidation of the alloys by boron and volatilization of the boric acid may be regarded to be complete below solidus. The most likely source of error is the iron or carbon contamination of commercial grade boron, and, in some instances, using improper techniques such as graphite for containing the sample material^(100, 101). Other considerations include the small ranges of homogeneity of the boride phases, limiting the observability of the true maximum to only a very narrow concentration range. Hence, a large number of alloys, closely spaced around the critical concentration, is necessary to ensure that the composition where maximum melting occurs has been included.

The solidus temperatures of metal-boron alloys, which are compiled in Tables 14 through 17 have been obtained on high purity alloy samples and confirmed by at least three measurements conducted at the congruently melting composition. The combined content of critical impurities (O + N + C + Si + iron metals) was usually less than 150 ppm, and in no instance exceeded 250 ppm; their effect can therefore be disregarded. For a detailed description of the sample materials, reference may be made to the series of documentary reports on the binary metal-boron systems⁽¹⁰⁵⁾.

D. MAXIMUM SOLIDUS TEMPERATURES OF THE TANTALUM-HAFNIUM MONOCARBIDE SOLID SOLUTION.

The melting point maxima in the solid solution series ZrC-TaC and HfC-TaC at a tantalum to hafnium (zirconium) ratio of about four, which were reported by C. Agte and H. Alterthum⁽²⁾ in 1930, have led to extensive theoretical speculations and considerations regarding the technical application of these alloys⁽³⁾. In investigations of the high temperature phase relationships in these systems^(106, 107), special attention was therefore devoted to the determination of the solidus temperatures of these compound solutions; the studies included the entire solidus envelope of the solution.

Table 14. Maximum Solidus Temperatures of Group IV Metal Borides

Boride	Literature Values	This Investigation, °C			Remarks
		T _{solid} (max.) [*]	Compos. At. % C	Average Reproducibility	
TiB	2060° (88) 1900 ± 50 (89)	2190 ± 30°	49	+ 25°	Peritect. dec.
TiB ₂	2900 ± 80° (89, 90, 5, 91, 92)	3225 ± 25°	66	+ 20°	Congruent melting
ZrB ₂	3190 ± 50° (93) 3040° (94, 95)	3245 ± 25°	66	+ 18°	Congruent melting
ZrB ₁₂	2680° (congr. melting)(94, 96)	2250 ± 50°	90	+ 40°	Peritect. dec.
HfB		2100 ± 25°	49	+ 20°	Peritect. dec.
HfB ₂	3100° (95, 53) 3240° (97) 3060° (5)	3380 ± 25°	66	+ 20°	Congruent melting

(*) Mean value and estimated overall uncertainty

Table 15. Maximum Solidus Temperatures of Group V Metal Borides

Boride	Literature Values	This Investigation, °C			Remarks
		T _{solid} (max) (*)	Compos. At. % C	Average Reproducibility	
V ₃ B ₂	2070° (98)	1900 ± 14°	40	± 12°	Peritectic. decomp.
VB	1900° (89)	2570 ± 20°	51	± 15°	Peritectic. decomp.
	2250° (98)				
V ₃ B ₅	2300° (98)	2610 ± 18°	56	± 15°	Peritectic. decomp.
VB ₂	~2400° (92, 89, 98)	2747 ± 20°	66	± 15°	Congruent melting
NbB	2280° (98)	2917 ± 16°	50	± 10°	Congruent melting
Nb ₃ B ₄	2700° (98)	2935 ± 20°	58	± 12°	Peritectic decomp.
NbB ₂	3000° (89, 92, 98)	3036 ± 20°	66	± 15°	Congruent melting
Ta ₂ B	1920° (98)	2417 ± 20°	30	± 15°	Peritectic. decomp.
	>2350° (97)				
TaB	2430° (98) >2800° (99)	3090 ± 20°	50	± 15°	Congruent melting
Ta ₃ B ₄	2650° (95)	3030 ± 35°	56	± 30°	Peritectic reaction
Ta ₂ B ₂	3100-3200° (89, 92, 98)	3037 ± 25°	60	± 30°	Congruent melting

(*) Mean value and estimated overall uncertainty

Table 16. Maximum Solidus Temperatures of Group VI Metal Borides

Boride	Literature Values	This Investigation, °C			Remarks
		T _{solid} (*)	Compos. At. % C	Average Reproducibility	
Mo ₂ B	2000° (100)	2280 ± 15°	34	± 12°	Peritectic decomp.
	2097-2142° (101)				
	2050° (102) (20 At% B)(103)				
β-MoB	2180° (100)	2600 ± 12°	50	± 8°	Congruent melting
	2325-2314° (101)				
MoB ₂	2100° (100)	2375 ± 25°	63	± 20°	Peritectic decomp.
Mo ₂ B ₅	-	2140 ± 20°	68	± 15°	Peritectic decomp.
W ₂ B	2770° (90, 3)	2670 ± 16°	33.5	± 12°	Congruent melting
β-WB	2860° (90, 3)	2665 ± 16°	48	± 12°	Congruent melting
W ₂ B ₅	~2300° (89)	2365 ± 15°	68	± 10°	Congruent melting

(*) Mean value and estimated overall temperature uncertainty

Table 17. Metal-Boride Eutectica

Eutectic Constituents	Literature Values	This Investigation, °C		
		T _{eut.} (*)	Eutect. Comp, At% B	Accuracy ± °C
β -Ti + TiB	1670 ± 25° (~14 At.% B) (88)	1540 ± 12°	7 ± 1	± 10°
β -Zr + ZrB ₂	1760° (22 At.% B)(94, 96, 3)	1660 ± 17°	12 ± 2	± 15°
β -Hf + HfB	1960° (104)	1880 ± 17°	13 ± 2	± 15°
V + V ₃ B ₂	1550° (~15 At.% B) (98)	1737 ± 10°	14 ± 1	± 8°
Nb + NbB	1600°C (~20 At.% B) (98)	2165 ± 15°	19 ± 2	± 10°
Ta + Ta ₂ B	1800° (19 At.% B) (98)	2385 ± 16°	23 ± 1	± 10°
Mo + Mo ₂ B	2000° (~8 At.% B) (100)	2175 ± 10°	23 ± 1	± 6°
W + W ₂ B	-	2600 ± 12°	27 ± 0.5	± 8°

(*) Mean value and estimated overall temperature uncertainty

A comparison of the solidus curves of the tantalum-hafnium monocarbide solution at fixed carbon defects of one, five, ten and thirteen atomic percent⁽¹⁰⁶⁾ indeed indicated a flat melting point maximum near TaC. However, the melting temperatures obtained at a given metal ratio and fixed carbon content do not necessarily coincide with the maximum solidus temperature of the solid solution at that particular metal exchange. To obtain the true maximum solidus line, therefore, we have to extract and combine the maximum solidus points for a series of alloys at fixed metal compositions, i.e. the carbon content of the alloys exhibiting the highest solidus temperature generally will vary with the metal exchange. In following these procedures, the data shown in Figure 15 for the (Ta, Hf)C_{1-x} solid solution, were extracted from measurements on over forty different alloy

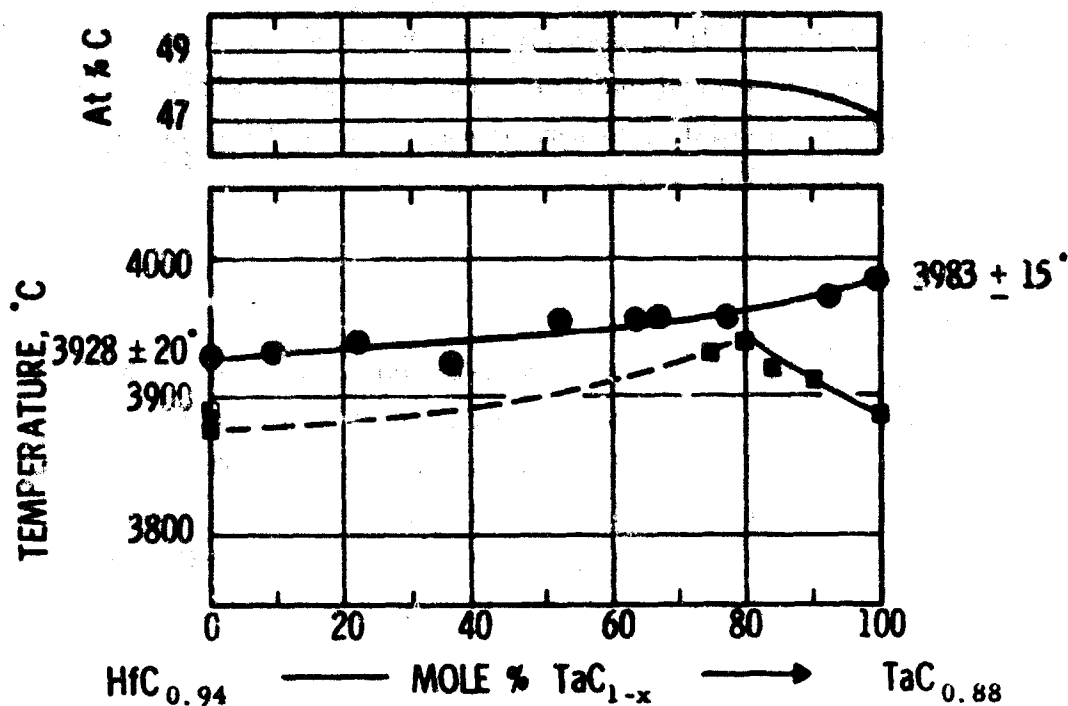


Figure 15. Maximum Solidus Temperatures for the Solid Solution $(\text{Ta, Hf})\text{C}_{1-x}$.

Top: Concentration Line of Maximum Melting (± 0.3 At% C)

■ C. Agte and H. Alterthum, 1930 (HfC-TaC)

● Our Measurements

● (Error limits based on reproducibility $\pm 25^\circ\text{C}$)

compositions, which covered the entire single phase band of the ternary solution. No melting point maximum occurs, and the maximum solidus temperatures vary smoothly between the congruent melting points of binary phases.

Two factors contribute to the appearance of the simulated melting point maxima at $X_c = \text{const}$: First, from the congruently melting binary alloy at 47 atomic percent carbon, the solidus temperatures of tantalum monocarbide drop rapidly as stoichiometry is approached. On the other hand, the concentration line of maximum melting shifts rapidly to higher carbon concentration upon substitution of tantalum by hafnium; hence, in alloy series

having a total carbon defect of one or two atomic percent, the binary tantalum-carbon alloys appear lower-melting than the ternary solid solution, thus explaining the previously observed maxima. The case of the zirconium-tantalum monocarbide solid solution is analogous, i.e. melting point maxima also do not exist in this system.

VII. DISCUSSION

The foregoing examples show the Pirani-technique as a very efficient and accurate tool for the determination of the solidus temperatures of refractory metallic substances. Chemical interaction problems virtually do not exist, and, provided that reasonable care has been taken in the preparation of the test specimens and in the calibration of the temperature measuring instruments, very little experience and skill is required to obtain reliable results.

Considering the disadvantages of the method in the conventional setup, probably the most serious one is its limitation to substances exhibiting metallic conductance; however, equipped with fast-response power feedback circuits to eliminate run-away problems, and with suitable preheating techniques to overcome the usually low conductance at low temperatures, the method may be adaptable to materials with negative temperature coefficients of resistance, such as semiconductors, or certain oxides. Another shortcoming of the method is associated with the difficulty of observing liquid formation in the presence of a large excess of solid. This occurs, for example, at the eutectic reaction isotherms in alloys located close to the boundaries of higher-melting phases. Thus, to obtain precise data for the isotherm, the measurements have to be carried out on alloys located at, or near, the isothermally melting compositions. Replacement of the visual temperature measurement method by photoelectric temperature transducers, capable of responding to minute temperature arrests, have been considered in this laboratory and have been shown effective to remedy this adverse effect.

The unmodified technique further is of limited use for the determination of the liquidus temperatures; the samples usually collapse before all of

the alloys, or at least that portion, where the pyrometer is focussed at, has transformed to liquid. Here again, by increasing the temperature gradient across the sample by increasing its cross-section, thermal analytical measurements carried out with photoelectric transducers, mounted on an automatic radiation tracking and focusing system, showed the possibility to overcome this specific shortcoming. For a description of this apparatus, however, reference may be made to a later publication.

In summarizing the discussion, we may conclude, that the available experience and the consistency of the data obtained by this method show the Pirani-technique, no doubt, to be the most reliable and convenient technique for the precise solidus temperatures of refractory metallic substances. With proper modifications, some of the shortcomings of the technique can be eliminated, and the capabilities extended to yield liquidus temperatures and allow thermal analytical measurements to be performed up to the melting temperatures of refractory alloys.

REFERENCES

1. M. Pirani and H. Alterthum: *Z. Electrochem.* 29 (1923), 5.
2. C. Agte and H. Alterthum: *Z. techn. Phys.* 11 (1930), 182.
3. Compare also the compilation of data in: R. Kieffer and F. Benesovsky, *Hartstoffe*, (Wien, Springer, 1963).
4. Compare, for example: W. Hume-Rothery, J. W. Christian, and W. B. Pearson; *Metallurgical Equilibrium Diagrams* (The Institute of Physics, London, 1952).
5. R. Kieffer, F. Benesovsky, and E. R. Honak: *Z. anorg. allg. Chem.* 268 (1952), 191.
6. F. H. Ellinger, *Trans. ASM* 31 (1953), 81.
7. W. P. Sykes, K. R. VanHorn, and C. M. Tucker: *Trans. AIME* 117 (1935), 173.
8. R. V. Sara: *J. Amer. Ceram. Soc.* 48 (1965), 243.
9. R. V. Sara: *Trans. AIME* 233 (1965), 1683.
10. G. V. Samsonov, V. S. Neshpor, and V. A. Ermakova: *Zur. Neorg. Chim.* 3 (1958), 868.
11. G. V. Samsonov and E. V. Petrash: *Metalloved. Obr. Metallov* 2 (1955), 19.
12. R. F. Goton: U.S. Patent No. 3,084,534 (1963).
13. S. Langer, General Atomic: Private Communication July 1961.
14. G. S. Rupert: *Rev. Sci. Instr.* 36, No. 11 (1965), 1629.
15. H. D. Heetderks, E. Rudy, and T. Eckert: *Planseeber. Pulvermet* 13 (1965), 105.
16. V. Nerses, E. J. Rapperport, and J. I. Klein in: WADD TR-60-132, Part III, Jan. 1964, p14.
17. R. F. Domagala and E. Heckenbach: *Rev. Sci. Instr.* 35 (12), (1964), 1663.
18. R. L. Bickerdike and G. Hughes: *J. Less Common Metals* 1 (1959), 42.
19. A. Taylor and H. B. Ryden: *J. Less Comm. Met.* 4 (1962), 451.
20. R. I. Jaffee and H. P. Nielson: *Trans. Amer. Inst. Min. Metall. Engrs.* 180 (1949), 180.

REFERENCES (Cont'd)

21. E.M. Savitski: Lecture given at Metallwerk Plansee AG, Reutte, Tirol, July 1960.
22. R.P. Adams and R.A. Beall: USBM Report of Invest. No. 6304 (Febr. 1963).
23. H. Kimura and Y. Sasaki: Trans. Jap. Inst. Met. 2 (1961), 98.
24. C.F. Zalabak: NASA Technical Note D-761 (March 1961).
25. A.G. Knapton, J. Savill, and R. Siddall: J. Less Comm. Met. 2 (1960), 357.
26. E. Rudy, St. Windisch, and Y.A. Chang: AFML-TR-65-2, Part I, Vol. I, (Jan 1965).
27. G.A. Geach and J.D. Summers-Smith: J. Inst. Met. 80 (1951), 143.
28. E.K. Storms and N.K. Krikorian: J. Phys. Chem. 64 (1960), 1471.
29. M.R. Null and W.W. Lozier: Research Mem. NRM-35, National Carbon Company (1961).
30. O. Krikorian: Paper presented at the Fall Instrumentation and Automation Conference, Los Angeles, Sept. 1961.
31. D.E. Hopping: Aerojet Measurements and Instrumentation Operations: Private Communication 1965 and 1966.
32. Work conducted under AF 33(615)-1249 at the Materials Research Laboratory, Sacramento, California. Report Series AFML-TR-65-2, Part I - IV (28 volumes, 1964 through 1966).
33. E. Rudy and D.P. Harmon: AFML-TR-65-2, Part I, Vol. V (Jan 1966).
34. R.A. Oriani and T.S. Jones: Rev. Sci. Instr. 25 (1954), 248.
35. D.J. Maykuth, H.R. Ogden, and R.I. Jaffee: J. Metals 5, 2251 (1953).
36. T.H. Schofield, and A.E. Bacon: J. Inst. Met. 82 (1953), 167.
37. D.K. Deardorff, E.T. Hayes: Trans. AIME 206 (1956), 509.
38. J.H. deBoer and J.D. Fast: Z. anorg. allg. Chemie 187 (1930), 193.
39. H.K. Adenstedt, J.R. Pequinof and J.M. Raymer: Trans. ASM 44 (1952), 990.
40. E.K. Storms and R.J. McNeal: J. Phys. Chem. 66 (1962), 1401.

REFERENCES (Cont'd)

41. A. Taylor and N.J. Doyle: *J. Less Common Met.* 7 (1964), 37.
42. T.H. Schofield: *J. Inst. Met.* 1956-1957, 372.
43. B. Riley: *J. Sci. Instr.* 41 (1964), 504.
44. J.H. Bechtold: *Acta Metallurgica* 3 (1955), 249.
45. W.G. Bradshaw and C.O. Mathews: "Properties of Refractory Materials. Collected Data and References", LMSD-2466 (1958).
46. G.W.C. Kaye and T.H. Laby: *Tables of Physical and Chemical Constants*, 12th Edit. (Longman's, London, 1959).
47. J. Hughes: *Assoc. Electr. Ind. Ltd., Research Lab. Report No. A497* (1955).
48. F. Jaeger and E. Rosenbohm: *Proc. Acad. Sci. Amsterdam* 36 (1933) 786.
49. C. Agte, H. Alterthum, K. Becker, G. Heyne, and K. Moers: *Z. anorg. allg. Chemie* 196 (1931), 129.
50. C.T. Sims, C.M. Craighead, and R.I. Jaffee: *Trans. AIME* (1955), 168.
51. A detailed description of the working procedures and the materials is given in the report series referenced under (32).
52. E. Friedrich and L. Sittig: *Z. anorg. allg. Chem.* 144 (1925), 169.
53. C. Agte and K. Moers: *Z. anorg. allg. Chemie* 198 (1931), 233.
54. G.A. Geach and F.O. Jones: 2nd Plansee Seminar, Reutte, Tirol, 1955 (*Plansee Proc.* 1955, 80).
55. P. Schwarzkopf and R. Kieffer: *Refractory Hard Metals* (MacMillan Comp., New York, 1953).
56. J.L. Engelke, F.A. Halden, and E.P. Farley: WADC-TR-59-654 (1960).
57. J. Farr: 1962. Work quoted in E.K. Storms, *Critical Review of Refractories*, LA-2942 (Aug 1962).
58. R.V. Sara, C.E. Lowell and R. T. Dolloff: WADD TR 60-143, Part IV (1963).
59. L.D. Brownlee: *J. Inst. Met.* 87 (1958), 58.
60. M.I. Copeland: USBM Progr. Rept. No. U-952 (June 1962), 14.
61. R.V. Sara and C.E. Lowell: WADD-TDR-60-143, Part V (1964).

REFERENCES (Cont'd)

62. O. Ruff and W. Martin: *Z. angew. Chem.* 25 (1912), 49.
63. M.G. Bowman: Paper presented at the V. Plansee Seminar, Reutte, Tirol, Austria, June 1964.
64. G.A. Geach and F.O. Jones: *Met. Abstr.* 24 (1957), 366.
65. R.T. Doloff and R.V. Sara: WADD TR 60-143 (1961), Part II.
66. R.V. Sara: *J.Amer.Ceram.Soc.* 48 (1965), 251.
67. W. Rostoker and A. Yamamoto: *Trans.Am.Soc.Met.* 46 (1954), 1136.
68. M.R. Nadler and C.P. Kempter: *J.Phys.Chem.* 64 (1960), 1468.
69. F.H. Ellinger: *Trans.Am.Soc. Met.* 31 (1943), 89.
70. D.S. Bloom and N.J. Grant: *Trans. AIME* 188 (1950), 41.
71. L. Ya. Markovskii, N.V. Vekshina, and R.A. Strikman: *Ogneupory*, 22 (1957), 42.
72. K. Hatsuta: *Sci.Rep. Tohoku Univ.* 10 (1932), 680.
73. G.A. Geach and F.O. Jones: *Plansee Proc.* 1955, 80.
74. T.C. Wallace, C.P. Gutierrez, and P.L. Stone: *J.Phys.Chem.* 67 (1963), 796.
75. M.R. Andrews and S. Dushman: *J.Franklin Inst.* 192 (1921), 545.
76. B.T. Barnes: *J.Phys.Chem.* 33 (1929), 688.
77. W.P. Sykes: *Trans.Am.Soc. Steel Treatm.* 19 (1930), 968.
78. O. Ruff and R. Wunsch: *Z.anorg.allg.Chem.* 85 (1914), 292.
79. I. Cadoff and J.P. Nielsen: *J.Metals* 5 (1955), 248.
80. F. Benesovsky and E. Rudy: *Planseeber Pulvermet.* 8 (1960), 66.
81. M.L. Pochon, C.R. McKinsey, R.A. Perkins and W.D. Forgeng in: "Reactive Metals: Vol.II, 327 (Interscience Publish. New York, 1959).
82. R.P. Elliott: *Trans.Am. Soc. Met.* 53 (1961), 13.
83. K.I. Portnoi, Yu.V. Levinski, and V.I. Fadajeva: *Izvest.Akad. Nauk SSSR, Otd. Tekhn. Nauk Met. i. Topliov* 2 (1961), 147.

REFERENCES (Cont'd)

84. E.K. Storms: unpublished work quoted in: E.K. Storms "Critical Review of Refractories" LA-2942 (1964).
85. P.G. Cotter and J.A. Kohn: J.Amer.Ceram.Soc. 37 (1954), 415.
86. N.H. Krikorian, 1962: Work quoted in E.K. Storms "Critical Review of Refractories," LA-2942 (1964).
87. H. Nowotny, E. Parthe, R. Kieffer, and F. Benesovsky: Mh.Chem. 85 (1954), 255.
88. A.E. Palty, H. Margolin, and J.P. Nielsen: Trans.Am.Soc.Met. 40 (1954), 312.
89. P. Schwarzkopf and F.W. Glaser: Z.Metallkde 44 (1953), 353.
90. F.R. Honak: Thesis, Techn. Hochschule Graz, 1951.
91. F.W. Glaser and W. Ivanick: Powd. Met. Bull. 6 (1953), 126.
92. B. Post, F.W. Glaser, and Moskowitz: Acta Met. 2 (1954), 20.
93. C. Agte: Thesis, Technische Hochschule Berlin, 1931.
94. F.W. Glaser and B. Post: Trans AIME 197 (1953), 1117.
95. K. Moers: Z. anorg.allg. Chemie 198 (1931), 262.
96. W. Schedler: Thesis, Technische Hochschule, Graz (1951).
97. F.W. Glaser, D.Moskowitz and B.W. Post: J.Metals 5 (1953), 1119.
98. H. Nowotny, F. Benesovsky, and R. Kieffer: Z.Metallkde, 50 (1959) 258.
99. J.M. Leitnaker: Rep. LA-2402 (1960).
100. R. Steinitz: Trans AIME 4 (1952), 148.
101. P.W. Gilles and B.D. Pollock: Trans AIME 5 (1953), 1537.
102. C. Yu-Chih, C. Tsiang-Lin, and W.Cheung-Hang: Sci.Sinica, 8 (1964) 1851.
103. Climax Molybdenum Co., Second Annual Report, 1951 (work quoted in M. Hansen, Constitution of Binary Alloys, McGraw Hill, New York, 1958).
104. L. Kaufmann and E.V. Clougherty: RTD-TDR-63-4096 (Part II, 1965).
105. E. Rudy and St. Windisch: AFML-TR-65-2, Part I, Vol. VII-X (1966), Vol. III (1965).

REFERENCES (Cont'd)

106. E. Rudy: AFML-TR-65-2, Part II, Vol. I (Sept. 1965).
107. D.P. Harmon and C.E. Brukl: AFML-TR-65-2, Part II, Vol. III (Nov. 1965).

Unclassified
Security Classification

DOCUMENT CONTROL DATA - R&D		
<i>(Security classification of title, body of abstract and indexing annotation must be entered when the overall report is classified)</i>		
1. ORIGINATING ACTIVITY (Corporate author) Materials Research Laboratory Aerojet-General Corporation Sacramento, California		2a. REPORT SECURITY CLASSIFICATION Unclassified
		2b. GROUP N.A.
3. REPORT TITLE Ternary Phase Equilibria in Transition Metal-Boron-Carbon-Silicon Systems Part III. Special Experimental Techniques. Vol. II. A Pirani-Furnace for the Precision Determination of the Melting Temperatures of Refractory Metallic		
4. DESCRIPTIVE NOTES (Type of report and inclusive dates)		Substances.
5. AUTHOR(S) (Last name, first name, initial) Rudy, E. Progulski, G.		
6. REPORT DATE May 1967	7a. TOTAL NO. OF PAGES 53	7b. NO. OF REFS 107
8a. CONTRACT OR GRANT NO. AF 33(615)-1249		8a. ORIGINATOR'S REPORT NUMBER(S) AFML-TR-65-2 Part III, Vol. II
a. PROJECT NO. 7350		
c. Task No. 735001		
d.		8b. OTHER REPORT NO(S) (Any other numbers that may be assigned this report) N.A.
10. AVAILABILITY/LIMITATION NOTICES This document is subject to special export controls, and each transmittal to foreign governments or foreign nationals may be made only with prior approval of Metals and Ceramics Division, Air Force Materials Labora- tory, Wright-Patterson Air Force Base, Ohio.		
11. SUPPLEMENTARY NOTES		12. SPONSORING MILITARY ACTIVITY AFML (MAMC) Wright-Patterson AFB, Ohio 45433
13. ABSTRACT An advanced design of a Pirani furnace is presented which allows the pre- cision determination of the melting temperatures of refractory metallic alloys. The method uses resistance heating of a specimen held between two water-cooled electrodes. The temperature of the phase change is determined optically with a disappearing-filament type micropyrometer at a small hole located in the center of the sample. Temperature calibration procedures, as well as methods and tools for the specimen preparation, are discussed. Measurements of the melting points of refractory metals and alloys, as well as of isothermal reaction temperatures in binary metal-carbon and metal-boron systems, are presented and compared with earlier data.		

DD FORM 1473
1 JAN 64

Unclassified
Security Classification

14. KEY WORDS	LINK A		LINK B		LINK C	
	ROLE	WT	ROLE	WT	ROLE	WT
High Temperature Experimental Techniques Melting Temperatures Refractory Materials						

INSTRUCTIONS

1. ORIGINATING ACTIVITY: Enter the name and address of the contractor, subcontractor, grantee, Department of Defense activity or other organization (*corporate author*) issuing the report.

2a. REPORT SECURITY CLASSIFICATION: Enter the overall security classification of the report. Indicate whether "Restricted Data" is included. Marking is to be in accordance with appropriate security regulations.

2b. GROUP: Automatic downgrading is specified in DoD Directive 5200.10 and Armed Forces Industrial Manual. Enter the group number. Also, when applicable, show that optional markings have been used for Group 3 and Group 4 as authorized.

3. REPORT TITLE: Enter the complete report title in all capital letters. Titles in all cases should be unclassified. If a meaningful title cannot be selected without classification, show title classification in all capitals in parentheses immediately following the title.

4. DESCRIPTIVE NOTES: If appropriate, enter the type of report, e.g., interim, progress, summary, annual, or final. Give the inclusive dates when a specific reporting period is covered.

5. AUTHOR(S): Enter the name(s) of author(s) as shown on or in the report. Enter last name, first name, middle initial. If military, show rank and branch of service. The name of the principal author is an absolute minimum requirement.

6. REPORT DATE: Enter the date of the report as day, month, year, or month, year. If more than one date appears on the report, use date of publication.

7a. TOTAL NUMBER OF PAGES: The total page count should follow normal pagination procedures, i.e., enter the number of pages containing information.

7b. NUMBER OF REFERENCES: Enter the total number of references cited in the report.

8a. CONTRACT OR GRANT NUMBER: If appropriate, enter the applicable number of the contract or grant under which the report was written.

8b, 8c, & 8d. PROJECT NUMBER: Enter the appropriate military department identification, such as project number, subproject number, system numbers, task number, etc.

9a. ORIGINATOR'S REPORT NUMBER(S): Enter the official report number by which the document will be identified and controlled by the originating activity. This number must be unique to this report.

9b. OTHER REPORT NUMBER(S): If the report has been assigned any other report numbers (either by the originator or by the sponsor), also enter this number(s).

10. AVAILABILITY/LIMITATION NOTICES: Enter any limitations on further dissemination of the report, other than those

imposed by security classification, using standard statements such as:

- (1) "Qualified requesters may obtain copies of this report from DDC."
- (2) "Foreign announcement and dissemination of this report by DDC is not authorized."
- (3) "U. S. Government agencies may obtain copies of this report directly from DDC. Other qualified DDC users shall request through _____."
- (4) "U. S. military agencies may obtain copies of this report directly from DDC. Other qualified users shall request through _____."
- (5) "All distribution of this report is controlled. Qualified DDC users shall request through _____."

If the report has been furnished to the Office of Technical Services, Department of Commerce, for sale to the public, indicate this fact and enter the price, if known.

11. SUPPLEMENTARY NOTES: Use for additional explanatory notes.

12. SPONSORING MILITARY ACTIVITY: Enter the name of the departmental project office or laboratory sponsoring (paying for) the research and development. Include address.

13. ABSTRACT: Enter an abstract giving a brief and factual summary of the document indicative of the report, even though it may also appear elsewhere in the body of the technical report. If additional space is required, a continuation sheet shall be attached.

It is highly desirable that the abstract of classified reports be unclassified. Each paragraph of the abstract shall end with an indication of the military security classification of the information in the paragraph, represented as (TS) (S) (C) or (U).

There is no limitation on the length of the abstract. However, the suggested length is from 150 to 225 words.

14. KEY WORDS: Key words are technically meaningful terms or short phrases that characterize a report and may be used as index entries for cataloging the report. Key words must be selected so that no security classification is required. Identifiers, such as equipment model designation, trade name, military project code name, geographic location, may be used as key words but will be followed by an indication of technical context. The assignment of links, roles, and weights is optional.